

Core charge of imidazolium annulated triphenylene derivatives induces discotic columnar mesomorphism

Shuai Chen,^a Hi Taing,^a Mohamed Ahmida,^a Hong Yi He,^a Aiden Carr,^a Heidi M. Muchall*^b and S. Holger Eichhorn*^a

Electronic Supplementary Information

1. Synthesis and Spectra	p. 2 – 23
2. Purity (HPLC, FT-IR)	p. 24 – 25
3. Mesomorphism	p. 26 – 34
4. Molecular Volume	p. 35
5. Computational Details and Data	p. 36 – 46
6. Cyclic voltammetry	p. 47 – 50
7. UV-vis spectra	p. 51
8. References for ESI	p. 52

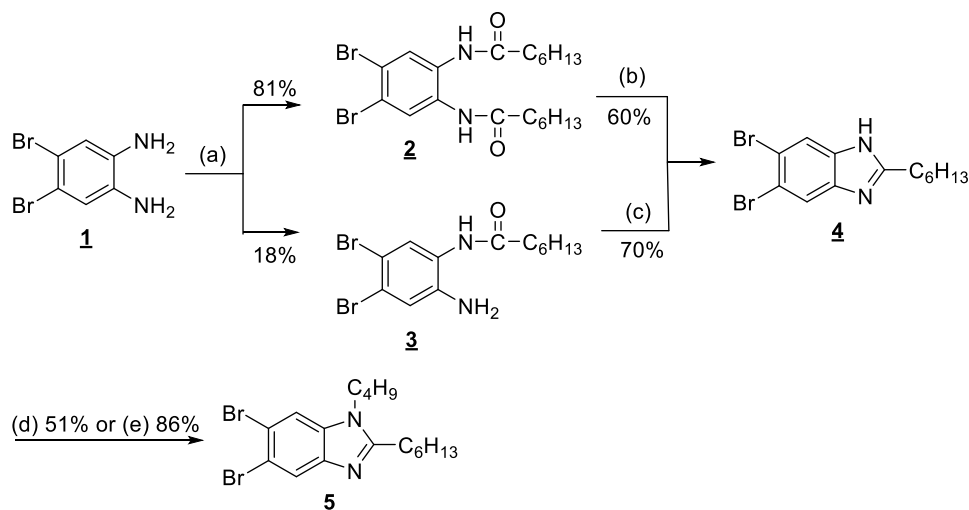
Synthesis and Characterization

Chemicals

All reagents and solvents were purchased from Sigma-Aldrich and Fluka Chemical Companies and used as purchased unless otherwise stated. Drying agents (MgSO_4 as well as 3 Å and 4 Å molecular sieves) were purchased from VWR. 1-Propanol and methanol were dried over 4 Å and 3 Å molecular sieves, respectively. Tetrahydrofuran and diethyl ether were obtained from a solvent purification system (Innovative Technology Inc. MA, USA, Pure-Solv 400). Silica gel 60 (35-70mesh ASTM, from EM Science, Germany) was used for column chromatography and Silica Gel 60 aluminum backed sheets (EM Science, Germany) for thin layer chromatography.

Instrumentation

^1H -NMR & ^{13}C -NMR spectra were obtained on Bruker NMR spectrometers (DRX 500 MHz, DPX 300 MHz and DPX 300 MHz with auto-tune). The residual proton signal of deuterated chloroform (CDCl_3) functioned as a reference signal. Multiplicities of the peaks are given as s = singlet, d = doublet, t = triplet, and m = multiplet. Coupling constants are given in Hz and only calculated for 1st-order coupling patterns. Data are presented in the following order (multiplicity, coupling constant, integration). Fourier Transform Infrared spectra (FT-IR) were obtained on a Bruker Vector 22. Relative peak intensities in IR are abbreviated as vs = very strong, s = strong, m = medium, w = weak, br = broad. Liquid samples were performed as films on potassium bromide plates and solid samples were run as potassium bromide pellets. Mass spectrometry measurements were performed by Kirk Green at the Regional Center for Mass Spectrometry (McMaster University) and Jiaxi Wang at the Mass Spectrometry and Proteomics Unit (Queen's University). HPLC was conducted on a Waters HPLC (binary pump 1525, UV-vis detector 2489, SunFire silica prep column (5 μm , 4.6 x 150 mm), Empower 3 software) at a flow rate of 1 mL/min.



Scheme S1. Synthesis of benzimidazole precursor. Compound **1** was prepared as reported previously.¹ Reaction Conditions: (a) 2.4 equiv. heptanoic acid, 1.2 equiv. DCC, 2.4 equiv. DIEA, DMF, 22-24 °C, 12 hrs; (b) 2.2 equiv. p-TsOH, toluene, reflux, 12 hrs, (c) AcOH, reflux, 5 hrs; (d) 1) 1.1 equiv. NaH, DMF, 24 °C, 1 hr; 2) 1.1 equiv. BrC₄H₉, 100 °C, 14 hrs; (e) 2 equiv. KOH, 2 equiv. K₂CO₃, 1.1 equiv. BrC₄H₉, 150 °C, 10 min, microwave.

Synthesis of N,N'-(4,5-dibromo-1,2-phenylene)diheptanamide (2) and N-(2-amino-4,5-dibromophenyl)heptanamide (3).² A solution of DCC (1.86 g, 9.02 mmol), DIEA (2.33 g, 18 mmol, dried by filtration through activated Al₂O₃) and 4,5-dibromobenzene-1,2-diamine **1** (2 g, 7.5 mmol) in dry CH₂Cl₂ (5 mL) was added to a solution of heptanoic acid (2.35 g, 18 mmol) in 100 mL DMF. The reaction was stirred at room temperature and stopped when **1** was fully consumed after about 8-12 hrs based on TLC analysis. The reaction mixture was filtered, the filtrate was diluted with CH₂Cl₂ (200 mL), extracted with 5% aqueous NaHCO₃ (6 x 50 mL, dried over MgSO₄, and concentrated in vacuum. Column chromatography of the residue (silica, Et₂O/Hexanes 2:1) gave two main fractions that yielded **2** (3 g, 81%) and **3** (0.5 g, 18%) as white solids.

Compound 2: ¹H NMR (500 MHz, CDCl₃): δ (ppm) 8.39 (s, 2H, HN), 7.55 (s, 2H, HAr), 2.31 (t, *J* = 5.0 Hz, 4H, (CO)CH₂), 1.66 (quintet, *J* = 7.1 Hz, 4H, CH₂), 1.33 (m, 12H, CH₂), 0.90 (t, *J* = 6.6 Hz, 6H, CH₃). ¹³C NMR (300 MHz, CDCl₃): δ (ppm) 172.69 (C=O), 130.69 (Ar), 126.22 (Ar), 125.54 (Ar), 37.36 (CH₂), 31.62 (CH₂), 29.02 (CH₂), 25.78 (CH₂), 22.58 (CH₂), 14.08 (CH₃). IR (KBr) ν_{max} (cm⁻¹): 3207, 2927, 2850, 1639, 1532, 1357, 1241. Melting point: 139 – 141 °C. HRMS ToF EI⁺ *m/e* for C₂₀H₃₀Br₂N₂O₂ calcd (M⁺) 488.0674, found 488.0667.

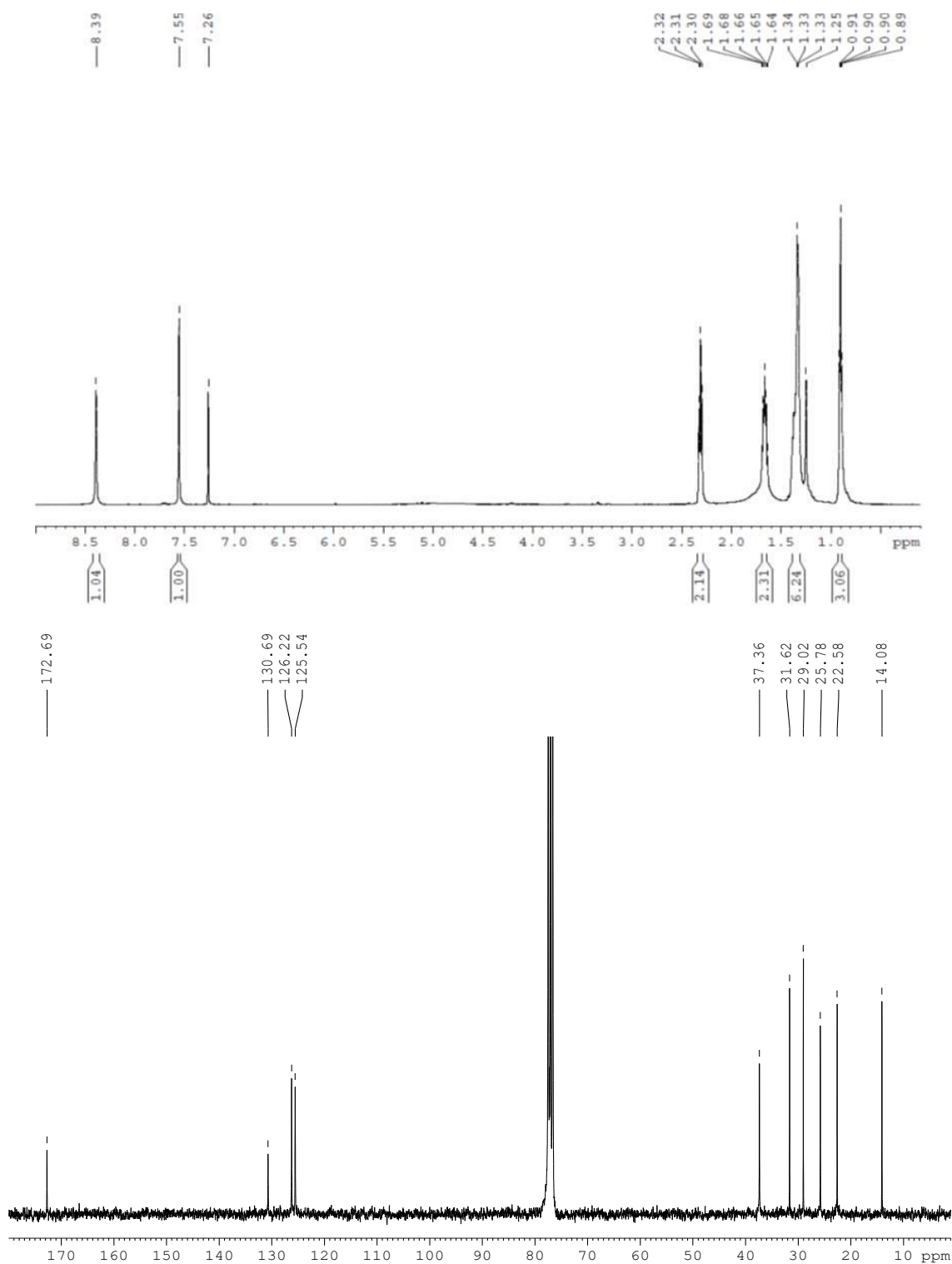


Figure S1. ^1H -NMR and ^{13}C -NMR of **2** in CDCl_3

Compound 3: ^1H NMR (300 Hz, CDCl_3): δ (ppm) 7.61 (s, 1H, NH), 7.40 (s, 1H, H_{Ar}), 6.99 (s, 1H, H_{Ar}), 3.90 (s_{broad} , 2H, NH_2), 2.33 (t, $J = 7.8$ Hz, 2H, $(\text{CO})\text{CH}_2$), 1.66 (quintet, $J = 7.5$ Hz, 2H, CH_2), 1.29 (m, 6H, CH_2), 0.88 (t, $J = 6.9$ Hz, 3H, CH_3). ^{13}C NMR (300 MHz, CDCl_3 plus 1 drop of DMSO): δ (ppm) 172.18 (C=O), 141.07 (C_{Ar}), 126.74 (C_{Ar}), 125.44 (C_{Ar}), 124.55 (C_{Ar}),

118.90 (C_{Ar}), 117.75 (C_{Ar}), 36.90 (CH₂), 31.58 (CH₂), 28.99 (CH₂), 25.72 (CH₂), 22.51 (CH₂), 14.06 (CH₃). HRMS ToF EI⁺ *m/e* for C₁₃H₁₈Br₂N₂O calcd (M⁺) 375.9786, found 375.9778.

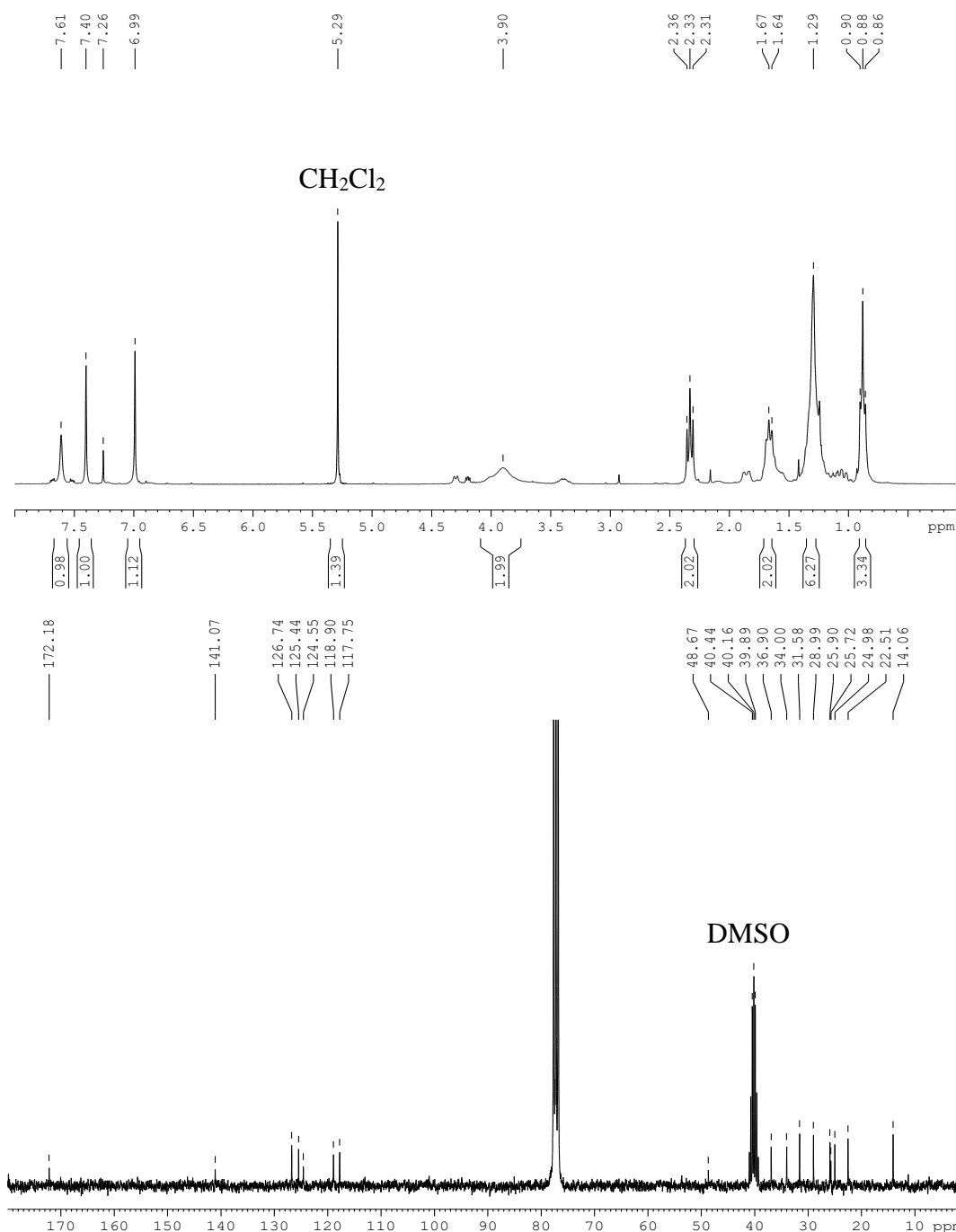
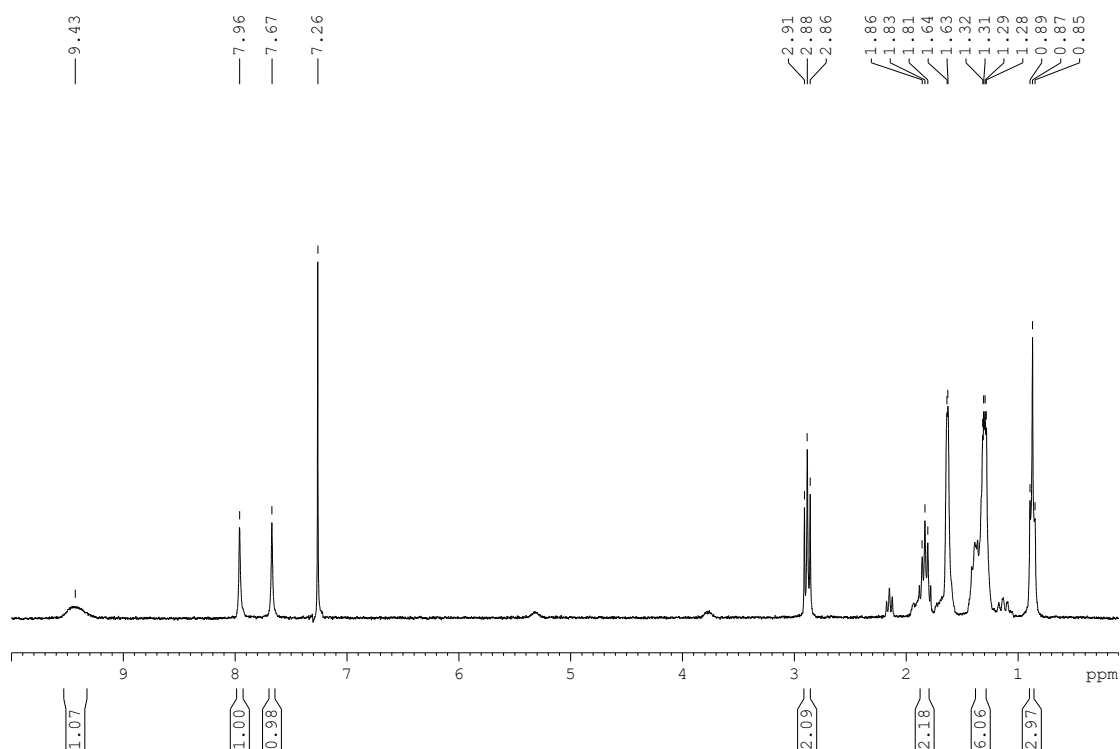


Figure S2. ¹H-NMR and ¹³C-NMR of **3** in CDCl₃. A drop of d₆-DMSO was added for ¹³C-NMR to increase solubility. Peaks at 48.67, 34.00, 25.90, and 24.98 ppm belong to unknown impurities.

Synthesis of 5,6-dibromo-2-hexyl-1H-benzo[d]imidazole (4**).**² p-toluenesulfonic acid (128 mg, 0.74 mmol) was added to a solution of **2** (165 mg, 0.34 mmol) in 50 mL toluene and the reaction mixture was heated to reflux for 10-12 hrs. The solvent was evaporated, and the residue was diluted with CH₂Cl₂ (100 mL) extracted with 5% aqueous NaHCO₃ (3 x 50 mL),

dried over MgSO₄ and concentrated. The residue was subject to column chromatography (silica, Et₂O/Hexanes, 2:1) to afford **4** as a white solid (73 mg, 60%).

Side-product **3** (500 mg, 1.24 mmol) was also converted into **4** by refluxing it in glacial acetic acid (10 mL) for 5 hrs. The solvent was evaporated in vacuum to give a solid residue that was dissolved in CH₂Cl₂ (100 mL), extracted with 5% aqueous NaHCO₃ (3 x 50 mL), and dried over MgSO₄. The concentrated solution was subject to column chromatography (silica, Et₂O/Hexanes, 2:1) to afford **4** as a white solid (330 mg, 70%). ¹H NMR (300 Hz, CDCl₃): δ (ppm) 9.43 (s_{broad}, 1H, NH), 7.96 (s, 1H, H_{Ar}), 7.67 (s, 1H, H_{Ar}), 2.89 (t, *J* = 7.5 Hz, 2H, CH₂), 1.83 (quintet, *J* = 7.5 Hz, 2H, CH₂), 1.31–1.28 (m, 6H, CH₂), 0.87 (t, *J* = 6.9 Hz, 3H, CH₃); ¹³C NMR (300 Hz, CDCl₃): δ (ppm) 157.30 (N-C=N), 138.47 (C_{Ar}), 119.08 (CH_{Ar}), 117.70 (CH_{Ar}), 31.46 (CH₂), 29.29 (CH₂), 29.02 (CH₂), 28.08 (CH₂), 22.50 (CH₂), 14.03 (CH₃). IR (KBr) ν_{max} (cm⁻¹): 3296, 2929, 2851, 1635, 1545, 1444, 1387, 1311, 1245. Melting point: 63-66 °C. HRMS ToF EI⁺ *m/e* for C₁₃H₁₆Br₂N₂ calcd (M⁺) 357.9680, found 357.9669.



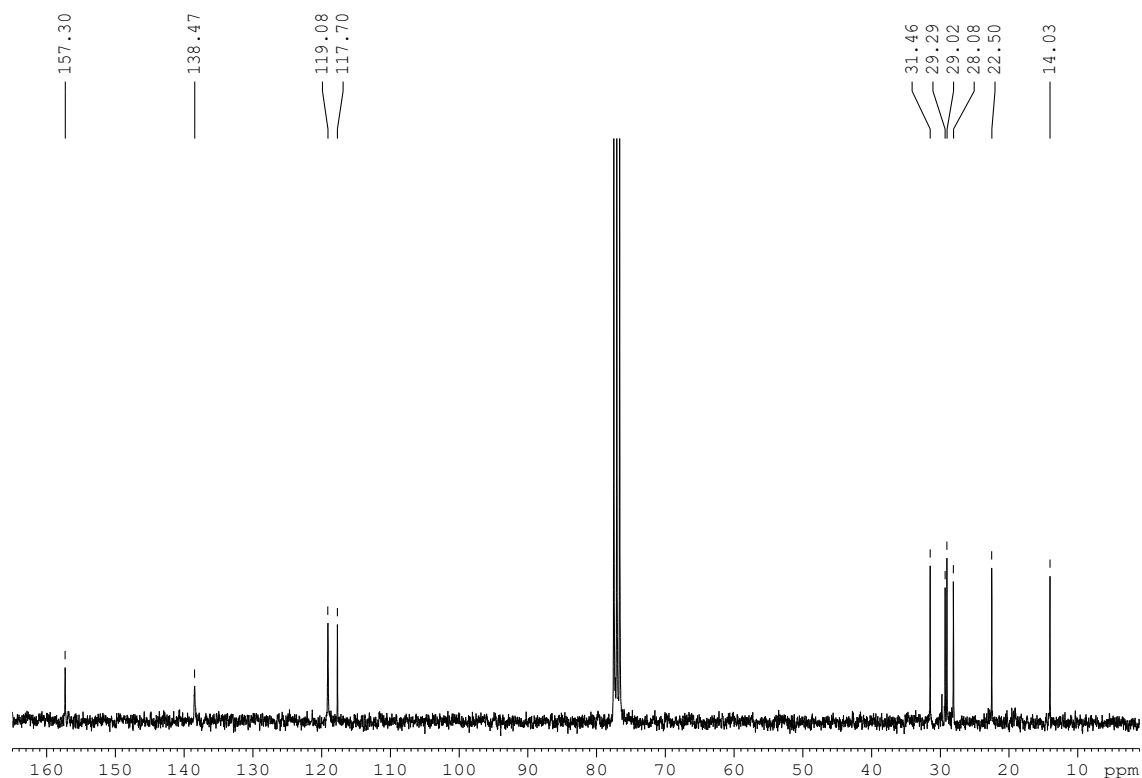


Figure S3. ^1H -NMR and ^{13}C -NMR of **4** in CDCl_3

Synthesis of 5,6-dibromo-1-butyl-2-hexyl-1*H*-benzo[*d*]imidazole (**5**).

Approach 1: NaH (60% dispersion in mineral oil) (25 mg, 0.68 mmol) was added at room temperature to a solution of **4** (224 mg, 0.62 mmol) in DMF (50 mL). After stirring for 1 hr, 1-bromobutane (94 mg, 0.68 mmol) was added. The mixture was heated to 100 °C for 10 hrs, cooled to room temperature, and then quenched by the addition of water (100 mL). The product was extracted with Et_2O (3 x 50 mL) and the organic layer was dried over MgSO_4 to give a yellow solution that was concentrated in vacuum and separated by column chromatography (silica, Et_2O /Hexanes 1:1). Compound **5** was obtained as a yellow oil (132 mg, 51%).

Approach 2: A mixture of **4** (100 mg, 0.28 mmol), KOH (31 mg, 0.56 mmol), K_2CO_3 (154 mg, 0.56 mmol) and 1-bromobutane (42 mg, 0.31 mmol) was heated to 150 °C for 10 min in a microwave oven (absorption level “high”). The reaction mixture was separated by column chromatography (silica, Et_2O /Hexanes 1:1) to afford **5** as a yellow oil (100 mg, 0.24 mmol, 86%).

^1H NMR (300 Hz, CDCl_3): δ (ppm) 7.93 (s, 1H, H_{Ar}), 7.53 (s, 1H, H_{Ar}), 4.00 (t, $J = 7.2$ Hz, 2H, NCH_2), 2.79 (t, $J = 7.8$ Hz, 2H, CH_2), 1.85 (quintet, $J = 7.8$ Hz, 2H, CH_2), 1.72 (quintet, $J = 7.8$ Hz, 2H, CH_2), 1.41–1.30 (m, 8H, CH_2), 0.95 (t, $J = 7.5$ Hz, 3H, CH_3), 0.87 (t, $J = 6.9$ Hz, 3H, CH_3). ^{13}C NMR (300 Hz, CDCl_3): δ (ppm) 157.25 (N-C=N), 143.21 (C_{Ar}), 135.34 (C_{Ar}), 123.63 (HC_{Ar}), 116.92 (C_{Ar}), 116.75 (C_{Ar}), 113.78 (HC_{Ar}), 43.77 (NCH_2), 31.89 (CH_2), 31.54 (CH_2),

29.23 (CH₂), 27.55 (two CH₂), 22.55 (CH₂), 20.21 (CH₂), 14.07 (CH₃), 13.75 (CH₃). IR (KBr) ν_{max} (cm⁻¹): 2955, 2928, 2855, 1680, 1608, 1506, 1445, 1393, 1302. HRMS ToF EI⁺ m/e for C₁₇H₂₄Br₂N₂ calcd (M⁺) 414.0306, found 414.0292.

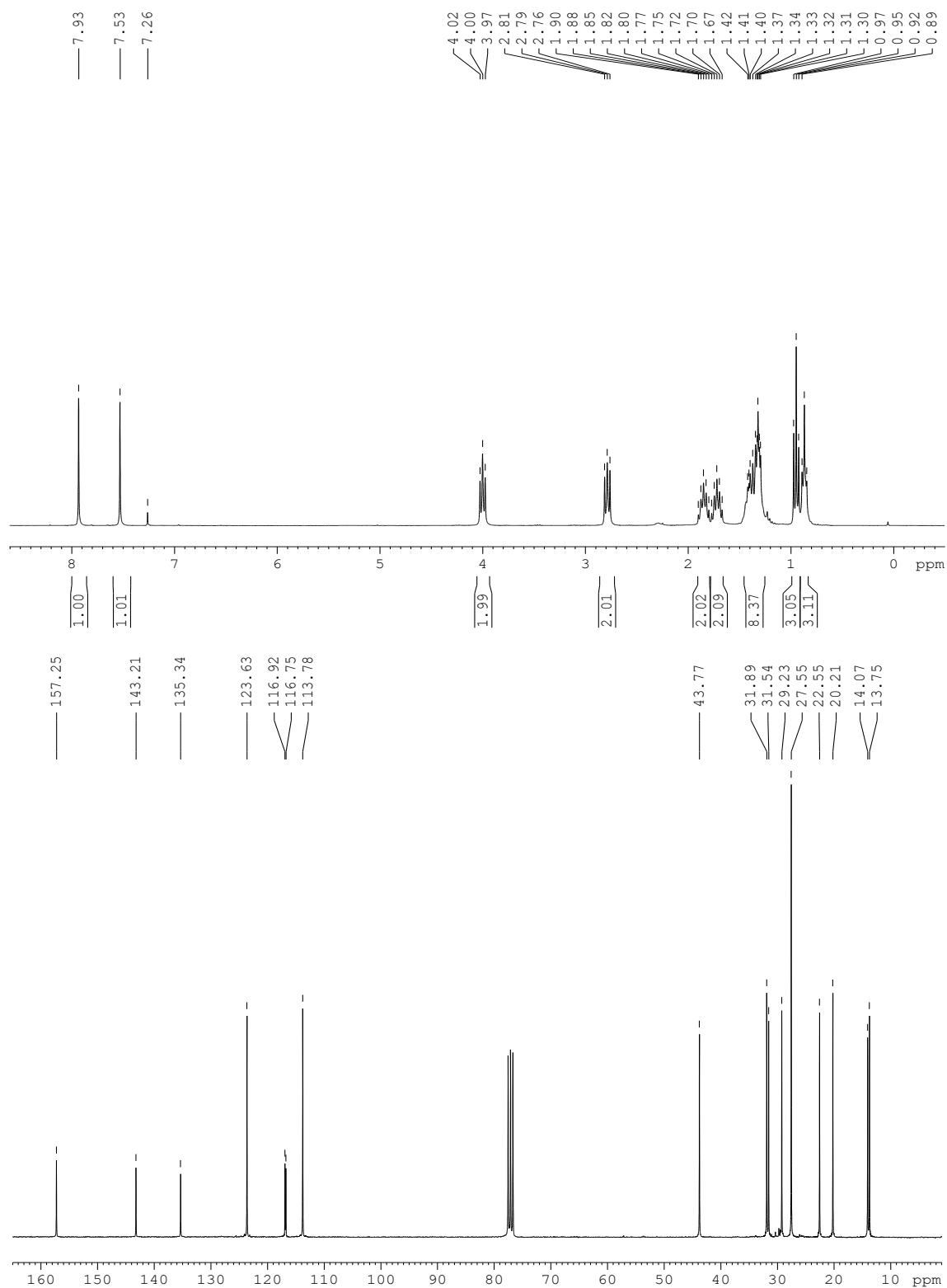
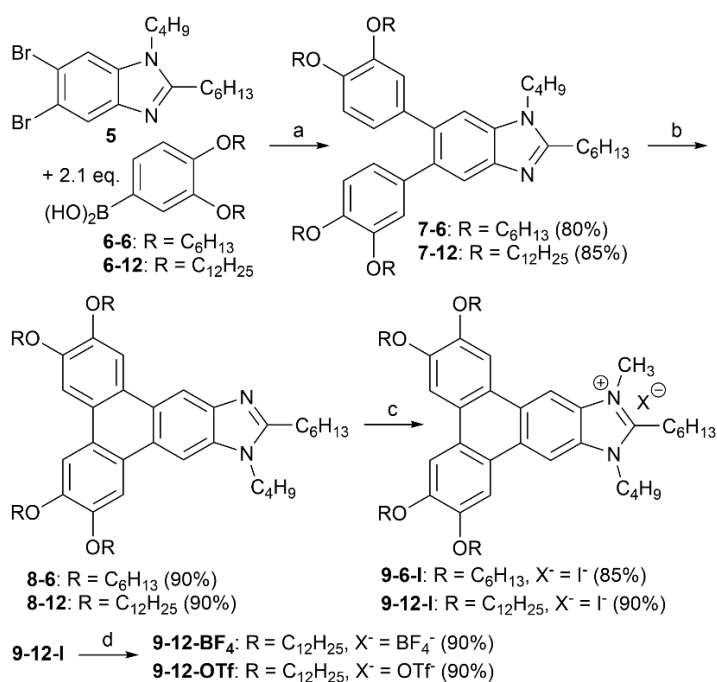


Figure S4. ¹H-NMR and ¹³C-NMR of **5** in CDCl₃



Scheme 1. Synthesis of imidazolium annulated triphenylene ionic liquid crystals.

Conditions: (a) 2.2 equiv. boronic acid, 2.2 eq. NaOH, 5 mol% Pd(PPh₃)₄, 1,4-dioxane, 80 °C, overnight; (b) 3 equiv. FeCl₃, CH₂Cl₂/MeNO₂ (1:1), 20-22 °C, 5 min c) 5 equiv. MeI, MeCN, 60-70 °C, 10 hrs; (d) 10 equiv. NaBF₄, CH₂Cl₂/H₂O/acetone, 20-22 °C, 15 hrs or 2 equiv. AgOTf, DCM/H₂O/acetone, 20-22 °C, 14 hrs.

Synthesis of 5,6-bis(3,4-bis(dodecyloxy)phenyl)-1-butyl-2-hexyl-1*H*-benzo[*d*]imidazole

(7-12). Pd(PPh₃)₄ (13 mg, 5 mol%) was added to an oxygen-free mixture of **5** (400 mg, 0.37 mmol), 3,4-bis(dodecyloxy)phenylboronic acid (**6-12**) (400 mg, 0.81 mmol), and NaOH (33 mg, 0.81 mmol) in 1,4-dioxane (30 mL) under dry nitrogen. The mixture was stirred for 20 hrs at 80 °C, extracted with CH₂Cl₂, and the combined organic layer was dried over Na₂SO₄ and concentrated. Column chromatography (silica, hexanes/Et₂O = 2:1) of the residue gave the product as a white solid (396 mg, 85%).

¹H-NMR (300 Hz, CDCl₃): δ (ppm) 7.77 (s, 1H, H_{Ar}), 7.30 (s, 1H, H_{Ar}), 6.79 (s_{broad}, 2H, H_{Ar}), 6.75 (s_{broad}, 2H, H_{Ar}), 6.62 (d, *J* = 8.1 Hz, 2H, H_{Ar}), 4.13 (t, *J* = 7.2 Hz, 2H, NCH₂), 3.96 (m, *J* = 6.6 Hz, two overlapping triplets, 4H, OCH₂), 3.67 (m, *J* = 6.6 Hz, two overlapping triplets, 4H, OCH₂), 2.90 (t, *J* = 7.5 Hz, 2H, CH₂, imine), 1.92 (quintet, *J* = 7.8 Hz, 2H, CH₂), 1.43-1.26 (m, 90H, CH₂), 0.98 (t, *J* = 7.5 Hz, 3H, CH₃), 0.88 (m, 15H, CH₃). ¹³C-NMR (300 Hz, CDCl₃): δ (ppm) 156.13 (N-C=N), 148.37 (C_{Ar}), 147.83 (C_{Ar}), 147.57 (C_{Ar}), 142.17 (C_{Ar}), 135.62 (C_{Ar}), 135.37 (C_{Ar}), 135.27 (C_{Ar}), 135.14 (C_{Ar}), 134.51 (C_{Ar}), 122.38 (C_{Ar}), 122.21 (C_{Ar}), 120.51 (C_{Ar}), 116.77 (C_{Ar}), 116.51 (C_{Ar}), 113.37 (C_{Ar}), 110.72 (C_{Ar}), 69.39 (OCH₂), 69.35 (OCH₂), 69.26 (OCH₂), 69.10 (OCH₂), 43.69 (NCH₂), 32.17 (NCH₃), 31.76 (CH₂), 31.68 (CH₂), 29.81 (CH₂), 29.45 (CH₂), 29.38 (CH₂), 29.19 (CH₂), 28.01 (CH₂), 27.71 (CH₂), 25.85 (CH₂), 25.80 (CH₂), 22.74 (CH₂), 20.36 (CH₂), 14.15 (CH₃), 13.89 (CH₃). IR (KBr) ν_{max} (cm⁻¹): 2920, 2851, 1603,

1578, 1513, 1465, 1249. Melting point: 42 – 44 °C. HRMS ToF MALDI⁺ *m/e* for C₇₇H₁₃₁N₂O₄ calcd (MH⁺) 1148.0108, found 1148.0127.

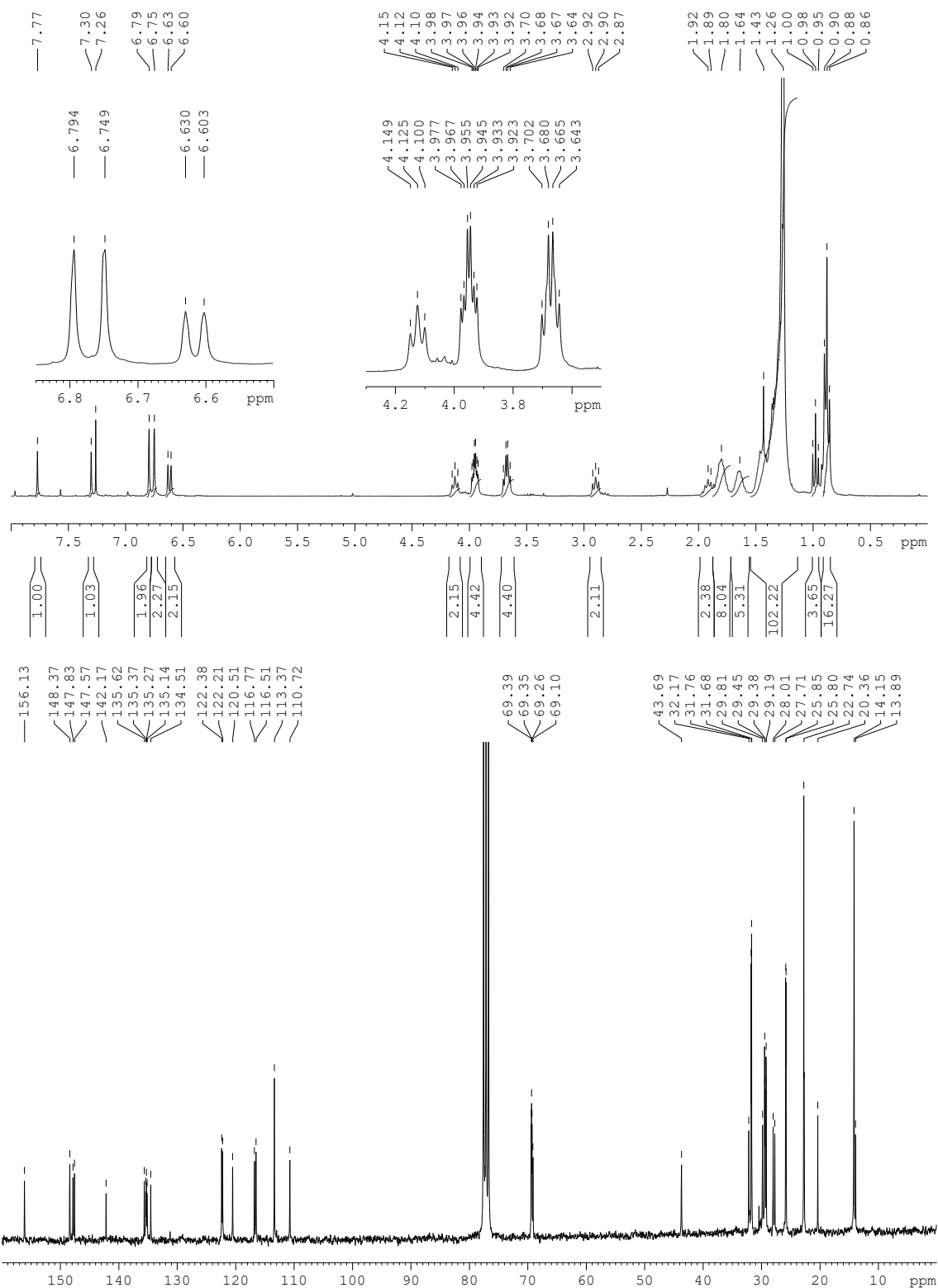


Figure S5. ¹H-NMR and ¹³C-NMR of **7-12** in CDCl₃.

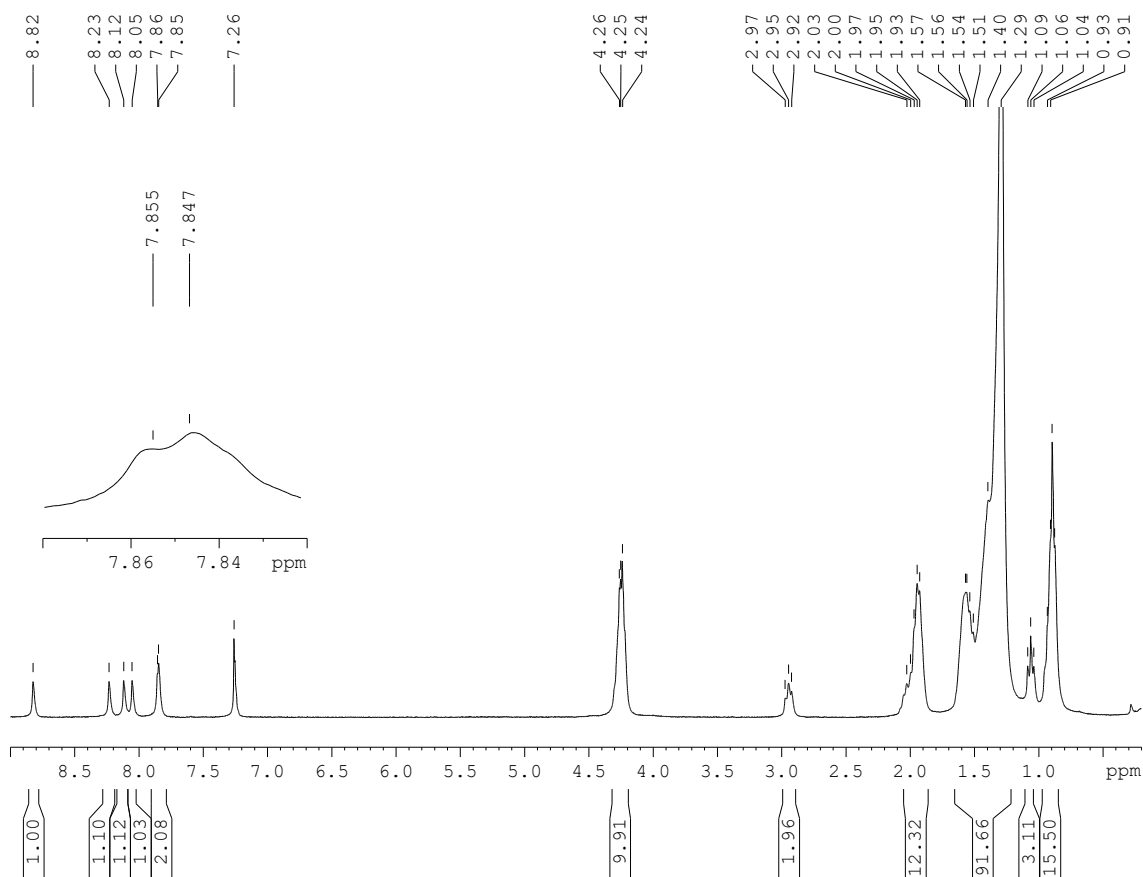
Synthesis of 10-butyl-2,3,6,7-tetrakis(dodecyloxy)-11-hexyl-10*H*-triphenyleno[2,3-*d*]imidazole (8-12**):** Compound **7-12** (714 mg, 0.62 mmol) was dissolved in a 1:1 mixture of

dry CH₂Cl₂ and dry MeNO₂ (20 mL). FeCl₃ (150 mg, 1.24 mmol) dissolved in MeNO₂ (5 mL) was added dropwise to the reaction mixture. After the addition of FeCl₃ was completed, the reaction mixture was stirred for 5 min and then quenched by the addition of 5 mL of dry MeOH. Finally, more MeOH was added until the crude product was precipitated out as a brown solid. Purification by column chromatography gave the product as an off-white solid (641 mg, 90%).

¹H-NMR (300 Hz, CDCl₃): δ (ppm) 8.82 (s, 1H, H_{Ar}), 8.23 (s, 1H, H_{Ar}), 8.12 (s, 1H, H_{Ar}), 8.05 (s, 1H, H_{Ar}), 7.86 (m, 1H, H_{Ar}), 7.85 (m, 1H, H_{Ar}), 4.25 (m, 10H, N,OCH₂), 2.95 (t, *J* = 7.5 Hz, 2H, CH₂, imine), 1.95 (m, 10H, CH₂), 1.56-1.29 (m, 82H, CH₂), 1.06 (t, *J* = 7.5 Hz, 3H, CH₃), 0.89 (m, 15H, CH₃).

¹³C-NMR (300 Hz, CDCl₃): δ (ppm) 157.81 (N-C=N), 149.55 (C_{Ar}), 149.37 (C_{Ar}), 148.77 (C_{Ar}), 135.08 (C_{Ar}), 125.33 (C_{Ar}), 125.03 (C_{Ar}), 124.39 (C_{Ar}), 124.21 (C_{Ar}), 122.96 (C_{Ar}), 112.25 (C_{Ar}), 108.82 (C_{Ar}), 108.08 (C_{Ar}), 107.58 (C_{Ar}), 106.95 (C_{Ar}), 101.61 (C_{Ar}), 70.29 (OCH₂), 70.16 (OCH₂), 69.69 (OCH₂), 69.10 (OCH₂), 43.49 (NCH₂), 31.98 (CH₂), 31.65 (CH₂), 29.73 (CH₂), 29.59 (CH₂), 29.42 (CH₂), 27.77 (CH₂), 27.50 (CH₂), 26.27 (CH₂), 26.20 (CH₂), 22.73 (CH₂), 22.61 (CH₂), 20.32 (CH₂), 14.13 (CH₃), 13.82 (CH₃).

IR (KBr) ν_{max} (cm⁻¹): 2917, 2849, 1616, 1519, 1466, 1430, 1387, 1260. Melting point: 75 – 79 °C. HRMS ToF EI⁺ *m/e* for C₇₇H₁₂₈N₂O₄ calcd (M⁺) 1144.9874, found 1144.9833.



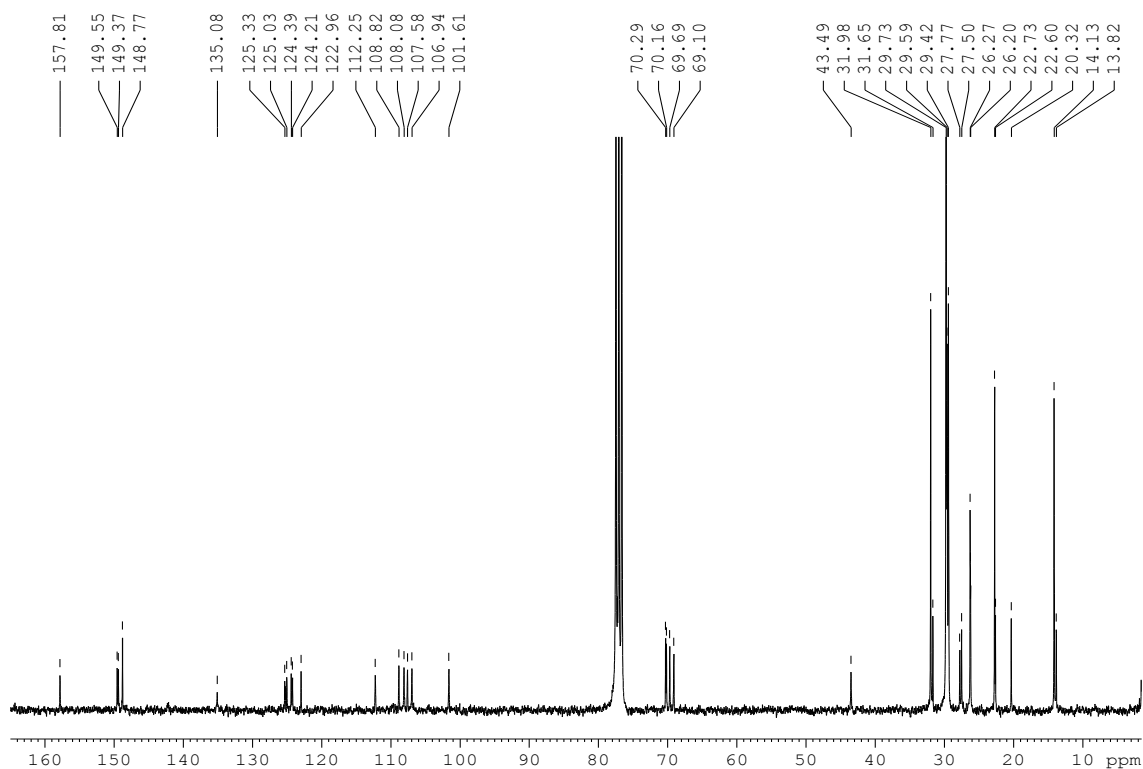


Figure S6. ^1H -NMR and ^{13}C -NMR of **8-12** in CDCl_3 .

Synthesis of 10-butyl-2,3,6,7-tetrakis(dodecyloxy)-11-hexyl-12-methyl-10H-triphenyleno[2,3-d]imidazol-12-ium iodide (9-12-I): Compound **8-12** (30 mg, 0.026 mmol) and iodomethane (18 mg, 0.13 mmol) were dissolved into 20 mL MeCN. The mixture was stirred at 60-70 °C for 10 hrs and then concentrated in vacuum. The residue was purified by column chromatography in $\text{CH}_2\text{Cl}_2/\text{MeOH}$ (100:1) to afford the product as a yellow solid (30 mg, 90%).

^1H -NMR (300 Hz, CDCl_3): δ (ppm) 9.00 (s, 1H, H_{Ar}), 8.96 (s, 1H, H_{Ar}), 8.43 (s, 1H, H_{Ar}), 8.41 (s, 1H, H_{Ar}), 7.80, 7.79 (s_{broad} , two overlapping singlets, 2H, H_{Ar}), 4.73 (t, $J = 5.4$ Hz, two overlapping triplets, 4H, OCH_2), 4.55 (s_{broad} , 2H, NCH_2), 4.27 (t, $J = 6.6$ Hz, two overlapping triplets, 4H, OCH_2), 3.98 (s, 3H, NCH_3), 2.03-1.96 (m, 12H, CH_2), 1.66-1.59 (m, 12H, CH_2), 1.45-1.27 (m, 70H, CH_2), 0.88 (m, 18H, CH_3). ^{13}C -NMR (300 Hz, CDCl_3): δ (ppm) 152.74 (N-C=N), 150.72 (C_{Ar}), 150.67 (C_{Ar}), 150.28 (C_{Ar}), 150.18 (C_{Ar}), 129.67 (C_{Ar}), 129.05 (C_{Ar}), 127.93 (H_{Ar}), 123.93 (C_{Ar}), 123.81 (C_{Ar}), 122.53 (C_{Ar}), 108.74 (C_{Ar}), 108.46 (C_{Ar}), 107.44 (C_{Ar}), 107.21 (C_{Ar}), 106.87 (C_{Ar}), 106.72 (C_{Ar}), 71.65 (OCH_2), 71.57 (OCH_2), 70.05 (two overlapping peaks, OCH_2), 46.62 (NCH_2), 34.60 (NCH_3), 31.99 (CH_2), 30.85 (CH_2), 29.81 (CH_2), 29.77 (CH_2), 29.66 (CH_2), 29.59 (CH_2), 29.44 (CH_2), 29.11 (CH_2), 26.53 (CH_2), 26.29 (CH_2), 22.74 (CH_2), 22.37 (CH_2), 19.97 (CH_2), 14.14 (CH_3), 13.96 (CH_3). IR (KBr) ν_{max} (cm^{-1}): 2918, 2849, 1612, 1520, 1457, 1388, 1264. HRMS ToF MALDI $^+$ m/e for $\text{C}_{78}\text{H}_{131}\text{IN}_2\text{O}_4$ calcd ($\text{M}^+ - \text{I}^-$) 1160.0108, found 1160.0128 and HRMS ToF MALDI $^-$ m/e for (I^-) calcd 126.9045, found 126.9049.

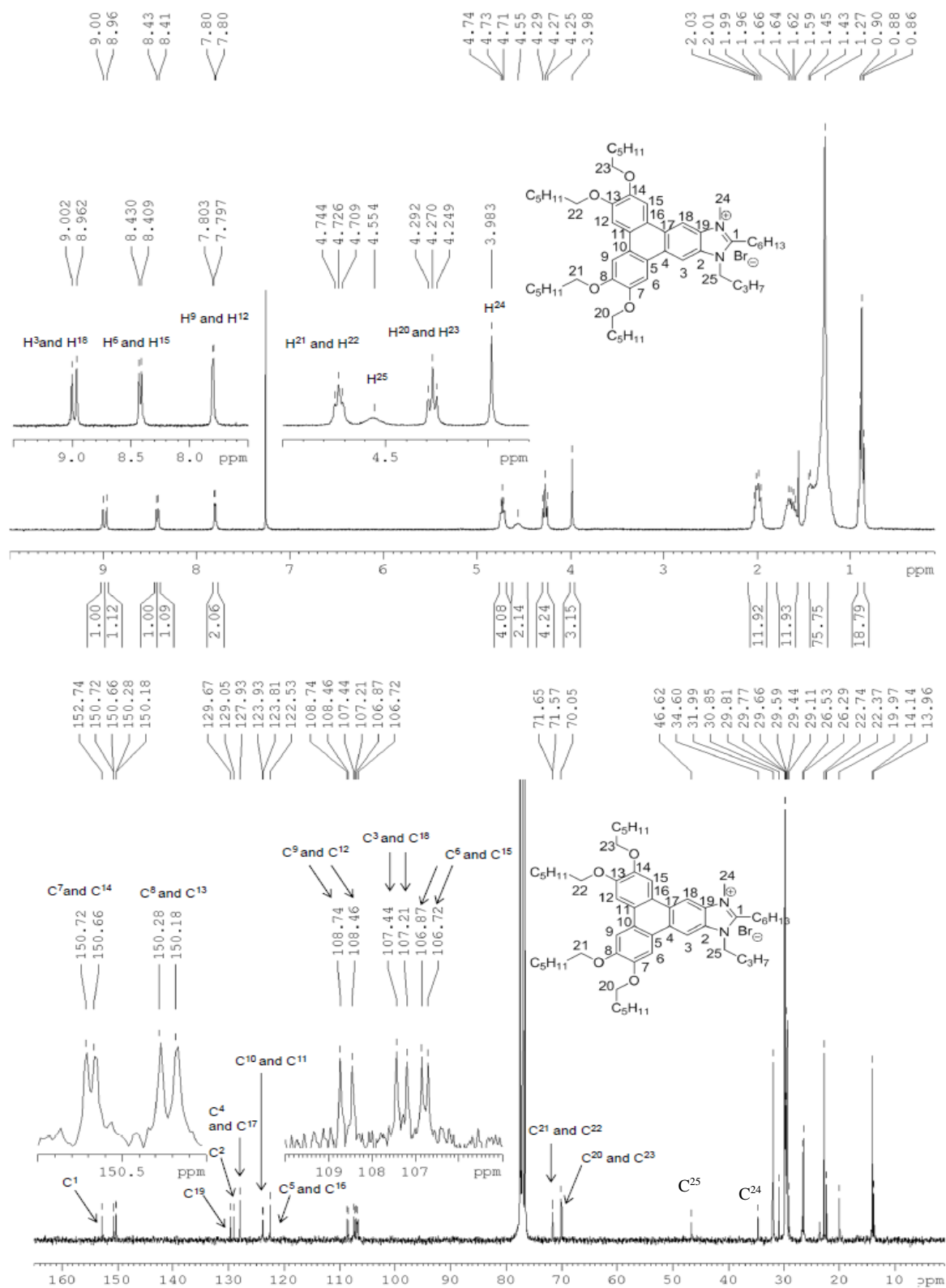


Figure S7. ¹H-NMR and ¹³C-NMR of **9-12-I** in CDCl₃. The structure is given with hexyloxy instead of dodecyloxy chains for simplicity.

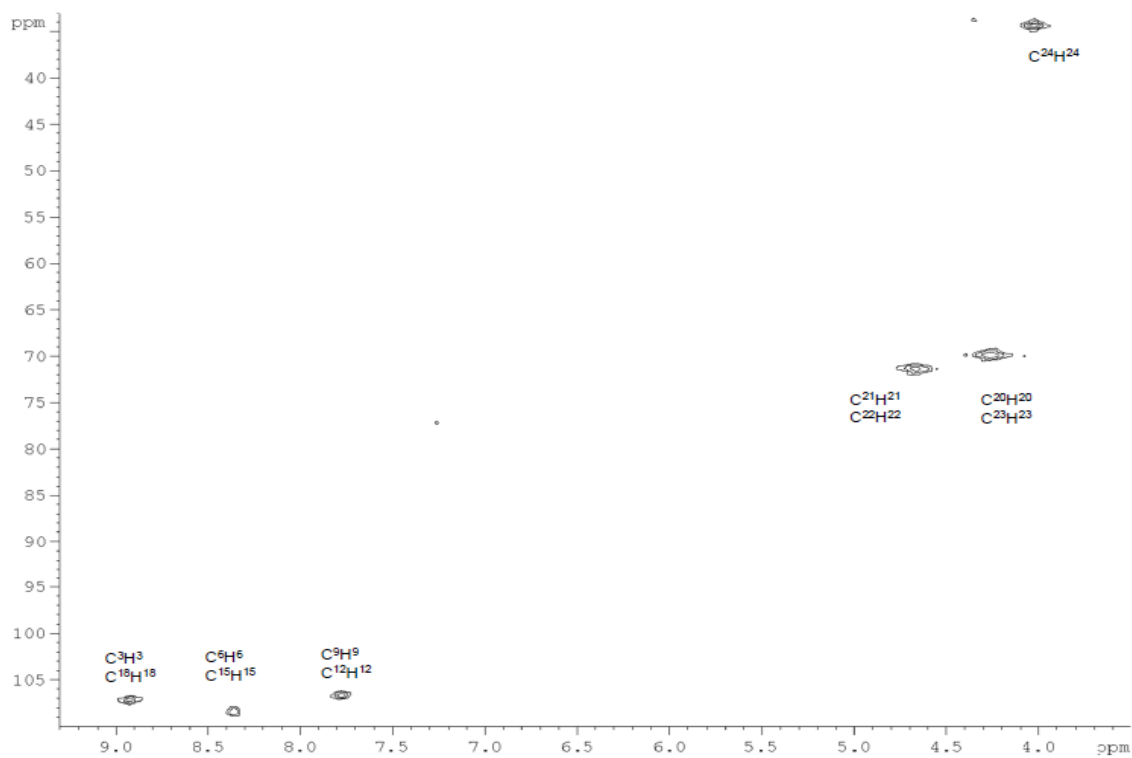


Figure S8. HMQC of **9-12-I** in CDCl₃

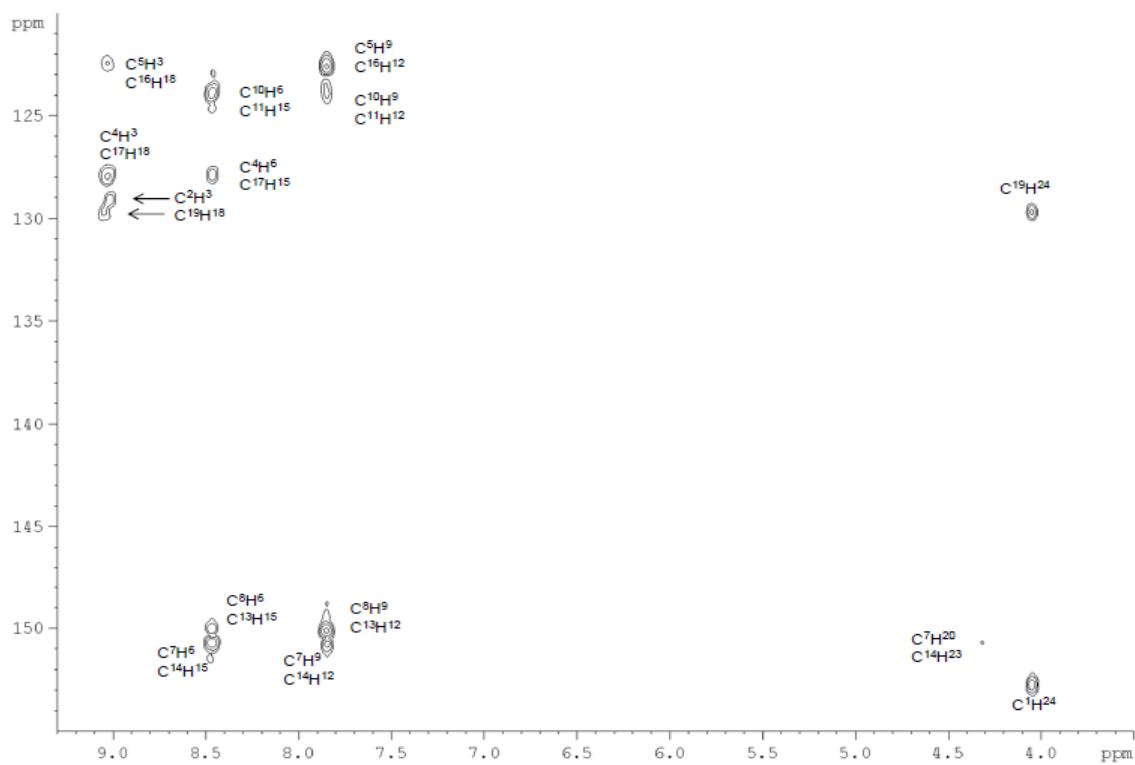


Figure S9. HMBC of **9-12-I** in CDCl₃

Synthesis of 10-butyl-2,3,6,7-tetrakis(dodecyloxy)-11-hexyl-12-methyl-10H-triphenyleno[2,3-d]imidazol-12-ium tetrafluoroborate (9-12-BF₄): Compound **9-12-I** (50 mg, 0.039 mmol) and 10 equivalents of NaBF₄ were dissolved in a mixture of CH₂Cl₂, Acetone, and H₂O until a clear solution was obtained. The solution was stirred for 16 hrs and extracted with CH₂Cl₂. The organic layer was extracted with deionized water, dried over MgSO₄, and concentrated. Purification by column chromatography (CH₂Cl₂/MeOH = 10:1) gave **9-12-BF₄** as a yellow-brown solid (43.6 mg, 90%).

¹H-NMR (300 Hz, CDCl₃): δ (ppm) 8.58 (s, 1H, H_{Ar}), 8.54 (s, 1H, H_{Ar}), 8.10 (s, 1H, H_{Ar}), 8.07 (s, 1H, H_{Ar}), 7.70 (s_{broad}, two overlapping singlets, 2H, H_{Ar}), 4.45 (m, *J* = 6.0 Hz, two overlapping triplets, 4H, O,NCH₂), 4.25 (m, *J* = 6.0 Hz, three overlapping triplets, 6H, O,NCH₂), 3.72 (s, 3H, NCH₃), 2.00-1.96 (m, 12H, CH₂), 1.64 (m, 12H, CH₂), 1.28 (m, 70H, CH₂), 0.89 (m, 18H, CH₃). ¹³C-NMR (300 Hz, CDCl₃): δ (ppm) 153.15 (N-C=N), 150.52 (C_{Ar}), 150.19 (C_{Ar}), 129.71 (C_{Ar}), 129.10 (C_{Ar}), 128.14 (C_{Ar}), 123.75 (C_{Ar}), 122.39 (C_{Ar}), 107.28 (C_{Ar}), 107.08 (C_{Ar}), 106.62 (C_{Ar}), 105.82 (C_{Ar}), 69.96 (OCH₂), 45.49 (NCH₂), 32.08 (NCH₃), 30.83 (CH₂), 29.92 (CH₂), 29.66 (CH₂), 29.54 (CH₂), 29.14 (CH₂), 26.52 (CH₂), 26.38 (CH₂), 22.83 (CH₂), 22.45 (CH₂), 19.76 (CH₂), 14.25 (CH₃), 14.05 (CH₃), 13.73 (CH₃). IR (KBr) ν_{max} (cm⁻¹): 2918, 2849, 1612, 1521, 1457, 1388, 1265. HRMS ToF MALDI⁺ *m/e* for C₇₈H₁₃₁BF₄N₂O₄ calcd (M⁺-BF₄⁻) 1160.0108, found 1160.0128 and HRMS ToF MALDI⁻ *m/e* for (BF₄⁻) calcd 87.0029, found 87.0028.

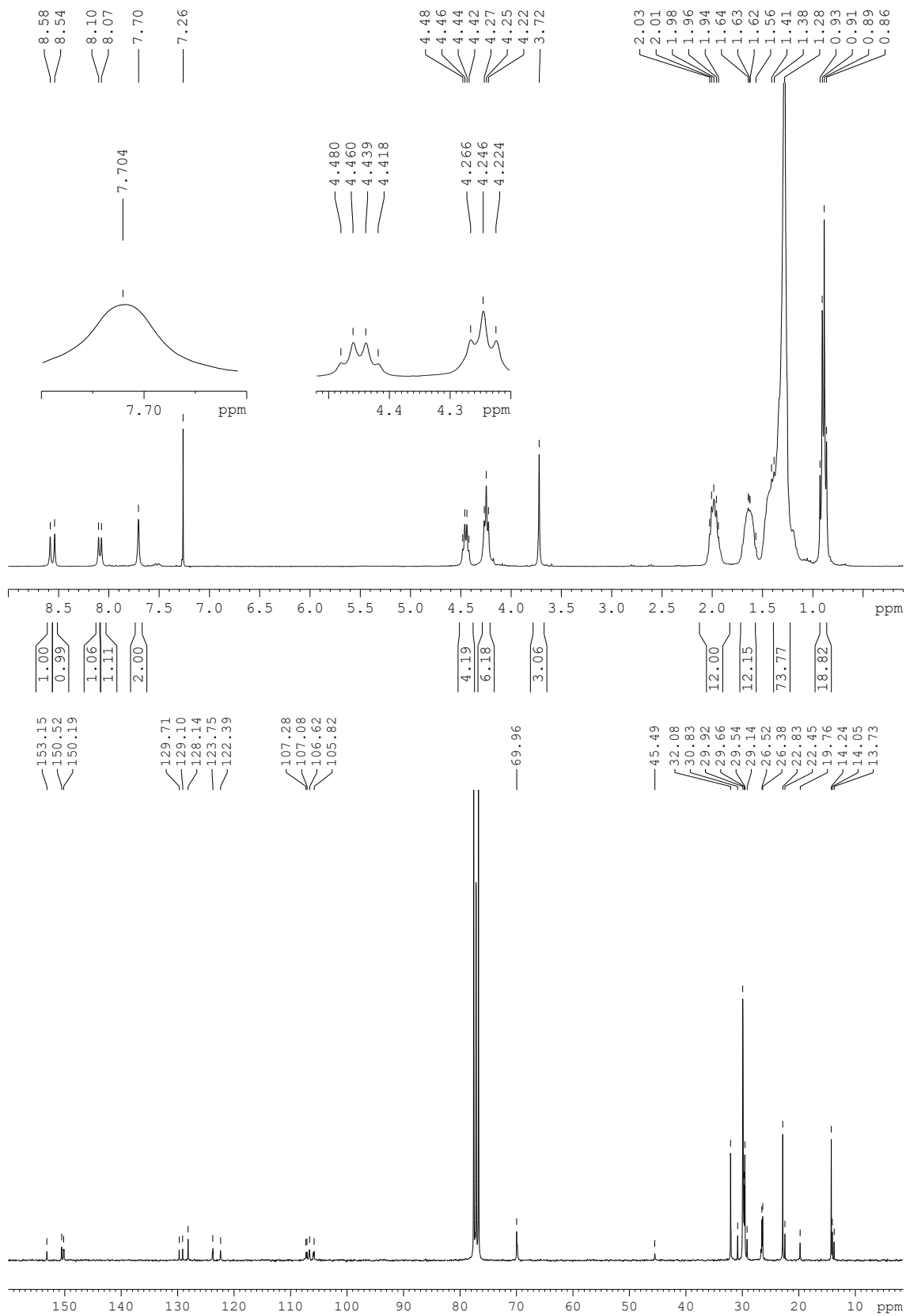


Figure S10. ¹H-NMR and ¹³C-NMR of **9-12-BF₄** in CDCl₃

Synthesis of 10-butyl-2,3,6,7-tetrakis(dodecyloxy)-11-hexyl-12-methyl-10H-triphenyleno[2,3-d]imidazol-12-ium trifluoromethanesulfonate (9-12-OTf): Compound **9-12-I** (50 mg, 0.039 mmol) and AgOTf (20 mg, 0.078 mmol) were dissolved in a mixture of CH₂Cl₂, Acetone and H₂O until a clear solution was obtained. The solution was stirred for 16 hrs at room temperature and then extracted with CH₂Cl₂. The combined organic layer was extracted with deionized water, dried over MgSO₄, and concentrated in vacuum. The residual was separated by column chromatography (CH₂Cl₂/MeOH (10:1)) to give **9-12-OTf** as a yellow-brown solid (45.8 mg, 90%).

¹H-NMR (300 Hz, CDCl₃): δ (ppm) 8.67 (s, 1H, H_{Ar}), 8.63 (s, 1H, H_{Ar}), 8.13 (s, 1H, H_{Ar}), 8.11 (s, 1H, H_{Ar}), 7.71 (s_{broad}, 2H, H_{Ar}), 4.42 (s_{broad}, three overlapping triplets, 6H, N,OCH₂), 4.23 (t, *J* = 6.0 Hz, two overlapping triplets, 4H, N,OCH₂), 3.86 (s, 3H, NCH₃), 2.16 (m, 2H, CH₂), 1.97 (m, 10H, CH₂), 1.78-1.61 (m, 12H, CH₂), 1.28 (m, 70H, CH₂), 0.89 (m, 18H, CH₃). ¹³C-NMR (300 Hz, CDCl₃): δ (ppm) 153.72 (N-C=N), 150.74 (C_{Ar}), 150.68 (C_{Ar}), 150.16 (C_{Ar}), 150.03 (C_{Ar}), 129.97 (C_{Ar}), 129.31 (C_{Ar}), 128.49 (C_{Ar}), 128.43 (C_{Ar}), 124.14 (C_{Ar}), 124.04 (C_{Ar}), 123.02 (C_{Ar}), 122.52 (C_{Ar}), 122.39 (C_{Ar}), 118.77 (C_{Ar}), 107.81 (C_{Ar}), 107.63 (C_{Ar}), 106.70 (C_{Ar}), 106.62 (C_{Ar}), 105.95 (C_{Ar}), 70.15 (OCH₂), 69.99 (OCH₂), 69.82 (OCH₂), 45.69 (NCH₂), 32.46 (NCH₃), 31.86 (CH₂), 30.86 (CH₂), 29.89 (CH₂), 29.76 (CH₂), 29.52 (CH₂), 29.53 (CH₂), 26.82 (CH₂), 26.52 (CH₂), 26.38 (CH₂), 23.24 (CH₂), 22.83 (CH₂), 22.47 (CH₂), 19.86 (CH₂), 14.24 (CH₃), 14.04 (CH₃), 13.73 (CH₃). IR (KBr) ν_{max} (cm⁻¹): 2918, 2850, 1612, 1520, 1457, 1435, 1387, 1263. HRMS ToF MALDI⁺ *m/e* for C₇₉H₁₃₁F₃N₂O₇S for (M⁺-OTf⁻) calcd 1160.0108, found 1160.0128 and HRMS ToF MALDI⁻ *m/e* for (OTf⁻) calcd 148.9520, found 148.9519.

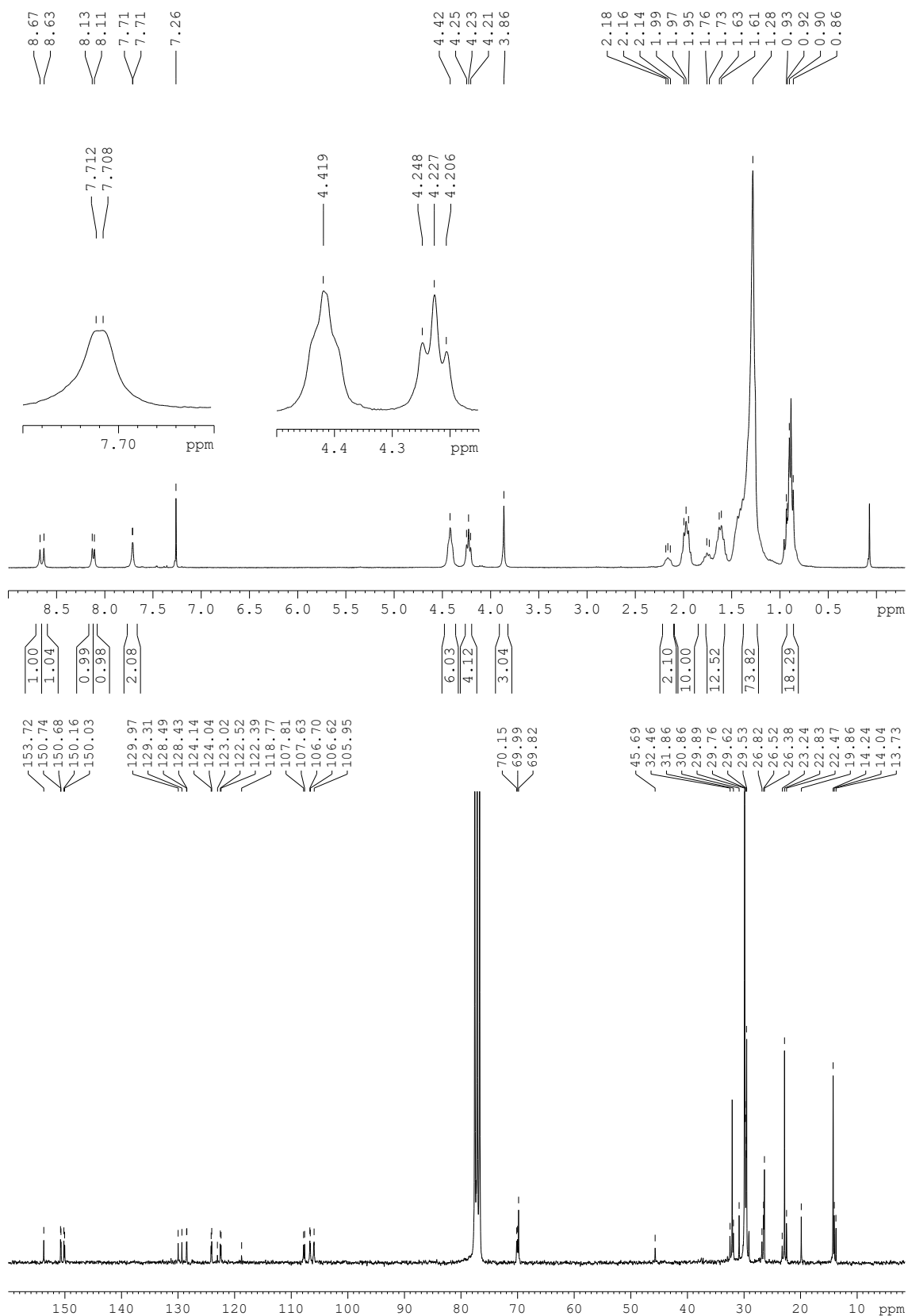
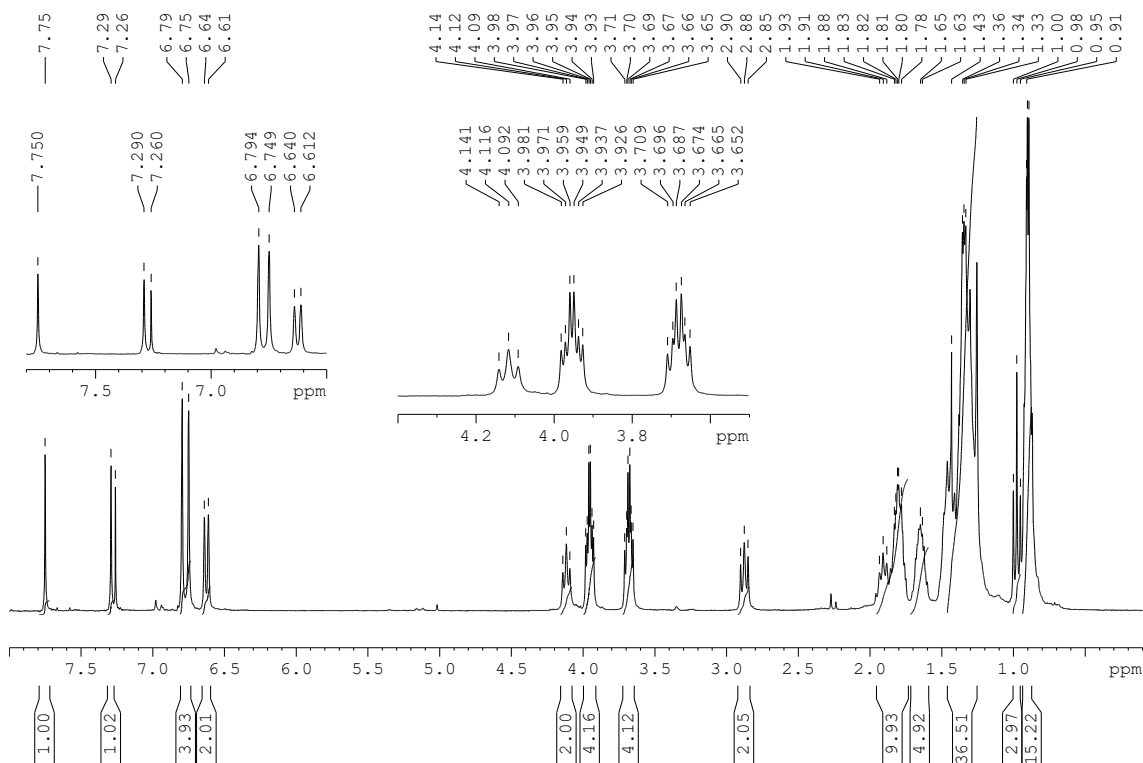


Figure S11. ¹H-NMR and ¹³C-NMR of 9-12-OTf in CDCl₃

Synthesis of 5,6-bis(3,4-bis(hexyloxy)phenyl)-1-butyl-2-hexyl-1*H*-benzo[*d*]imidazole (7-6): Pd(PPh₃)₄ (36 mg, 5 %mol) was added to a mixture of **5** (262 mg, 0.63 mmol), 3,4-bis(hexyloxy)phenylboronic acid **6-6** (445 mg, 1.39 mmol), and Cs₂CO₃ (451 mg, 1.39 mmol) in DMF/toluene (30 mL, 1:1) under dry nitrogen. The mixture was stirred for 16 hrs at 90 °C, extracted with CH₂Cl₂, and the combined organic layer was dried over Na₂SO₄ and concentrated. This solution was subject to column chromatography on silica gel (hexanes/Et₂O (2:1)) to give a colorless oil **7-6** (420 mg, 80%).

¹H-NMR (300 Hz, CDCl₃): δ (ppm) 7.75 (s, 1H, H_{Ar}), 7.29 (s, 1H, H_{Ar}), 6.79-6.75 (d, overlapping singlet and doublet, *J* = 13.5 Hz, 4H, H_{Ar}), 6.63 (d, *J* = 8.4 Hz, 2H, H_{Ar}), 4.12 (t, *J* = 7.5 Hz, 2H, NCH₂), 3.96 (m, two overlapping triplets, *J* = 6.6 Hz, 4H, OCH₂), 3.67 (m, two overlapping triplets, *J* = 6.6 Hz, 4H, OCH₂), 2.88 (t, *J* = 7.5 Hz, 2H, CH₂, imine), 1.91-1.78 (m, 10H, CH₂), 1.65 (m, 6H, CH₂), 1.43-1.33 (m, 28H, CH₂), 0.98 (t, *J* = 7.2 Hz, 3H, CH₃), 0.90 (m, 15H, CH₃).
¹³C-NMR (300 Hz, CDCl₃): δ (ppm) 156.13 (N-C=N), 148.37 (C_{Ar}), 147.83 (C_{Ar}), 147.57 (C_{Ar}), 142.17 (C_{Ar}), 135.62 (C_{Ar}), 135.37 (C_{Ar}), 135.27 (C_{Ar}), 135.14 (C_{Ar}), 134.51 (C_{Ar}), 122.38 (C_{Ar}), 122.21 (C_{Ar}), 120.51 (C_{Ar}), 116.77 (C_{Ar}), 116.51 (C_{Ar}), 113.37 (C_{Ar}), 110.72 (C_{Ar}), 69.39 (OCH₂), 69.35 (OCH₂), 69.26 (OCH₂), 69.10 (OCH₂), 43.69 (NCH₂), 32.17 (NCH₃), 31.76 (CH₂), 31.68 (CH₂), 29.81 (CH₂), 29.45 (CH₂), 29.38 (CH₂), 29.19 (CH₂), 28.01 (CH₂), 27.71 (CH₂), 25.85 (CH₂), 25.80 (CH₂), 22.74 (CH₂), 20.36 (CH₂), 14.15 (CH₃), 13.89 (CH₃). IR (KBr) ν_{max} (cm⁻¹): 2927, 2858, 1602, 1508, 1454, 1245. HRMS ToF EI⁺ *m/e* for C₅₃H₈₂N₂O₄ calcd (M⁺) 810.6275, found 810.6289.



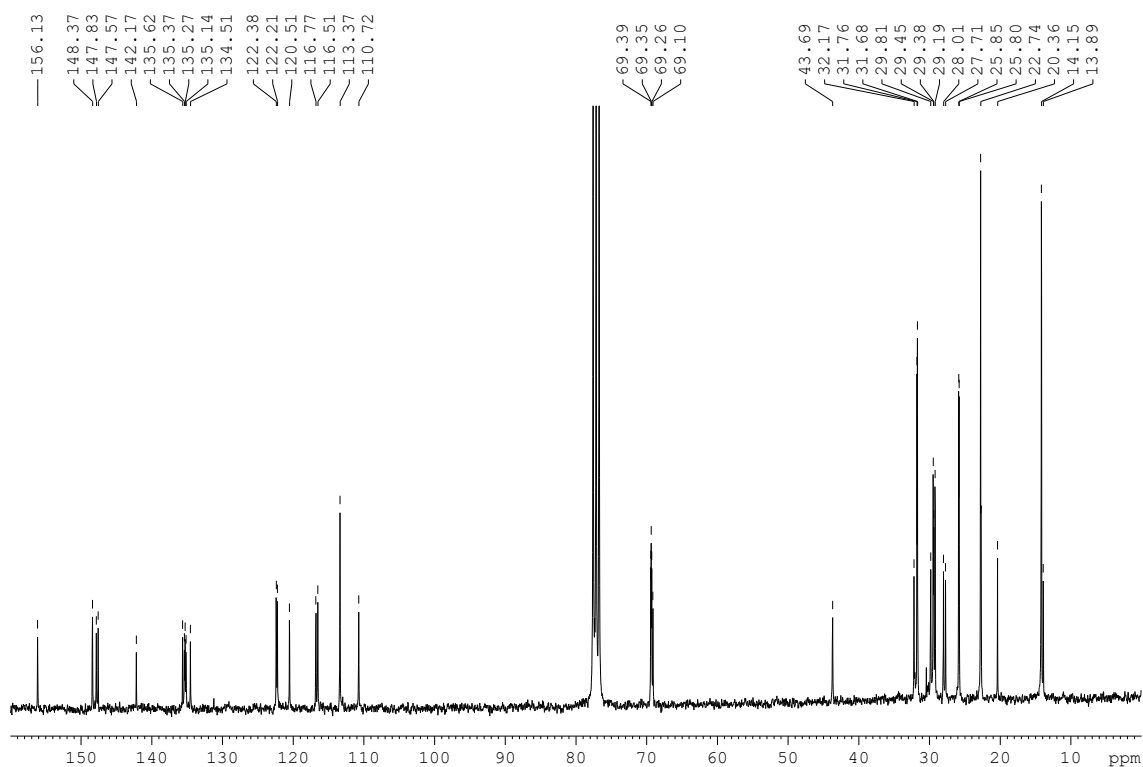


Figure S12. $^1\text{H-NMR}$ and $^{13}\text{C-NMR}$ of **7-6** in CDCl_3

Synthesis of 10-butyl-11-hexyl-2,3,6,7-tetrakis(hexyloxy)-10H-triphenyleno[2,3-d]imidazole (8-6): **7-6** (290 mg, 0.36 mmol) was dissolved in a mixture of $\text{CH}_2\text{Cl}_2/\text{MeNO}_2$ 1:1. FeCl_3 (174 mg, 1.07 mmol) dissolved in a minimum volume of MeNO_2 was injected into solution dropwise. After stirring for 5 min, 5 mL dry MeOH was added to quench the reaction. A larger volume of MeOH was added to fully precipitate out the product as a white solid **8-6** (260 mg, 90%).

$^1\text{H-NMR}$ (300 Hz, CDCl_3): δ (ppm) 8.83 (s, 1H, H_{Ar}), 8.23 (s, 1H, H_{Ar}), 8.10 (s, 1H, H_{Ar}), 8.05 (s, 1H, H_{Ar}), 7.84 (s, 1H, H_{Ar}), 7.83 (s, 1H, H_{Ar}), 4.25 (m, 10H, N,OCH_2), 2.94 (t, $J = 7.5$ Hz, 2H, CH_2 , imine), 1.95 (m, 10H, CH_2), 1.56-1.39 (m, 34H, CH_2), 1.05 (t, $J = 7.5$ Hz, 3H, CH_3), 0.93 (m, 15H, CH_3). $^{13}\text{C-NMR}$ (300 Hz, CDCl_3): δ (ppm) 157.87 (N-C=N), 149.51 (C_{Ar}), 149.33 (C_{Ar}), 148.74 (C_{Ar}), 142.35 (C_{Ar}), 135.15 (C_{Ar}), 125.27 (C_{Ar}), 125.17 (C_{Ar}), 125.04 (C_{Ar}), 124.35 (C_{Ar}), 124.22 (C_{Ar}), 122.93 (C_{Ar}), 112.28 (C_{Ar}), 108.76 (C_{Ar}), 108.03 (C_{Ar}), 107.54 (C_{Ar}), 106.88 (C_{Ar}), 101.58 (C_{Ar}), 70.24 (OCH_2), 70.13 (OCH_2), 69.67 (OCH_2), 69.06 (OCH_2), 43.47 (NCH_2), 31.99 (CH_2), 31.74 (CH_2), 31.69 (CH_2), 29.74 (CH_2), 29.59 (CH_2), 29.50 (CH_2), 29.35 (CH_2), 29.33 (CH_2), 27.80 (CH_2), 27.49 (CH_2), 25.91 (CH_2), 25.88 (CH_2), 22.71 (CH_2), 22.61 (CH_2), 20.33 (CH_2), 14.10 (CH_3), 13.90 (CH_3). IR (KBr) ν_{max} (cm^{-1}): 2922, 2854, 1615, 1519, 1455, 1430, 1388, 1257, 1163. Melting point: 69–72 °C. HRMS ToF EI^+ m/e for $\text{C}_{53}\text{H}_{80}\text{N}_2\text{O}_4$ calcd (M^+) 808.6118, found 808.6133.

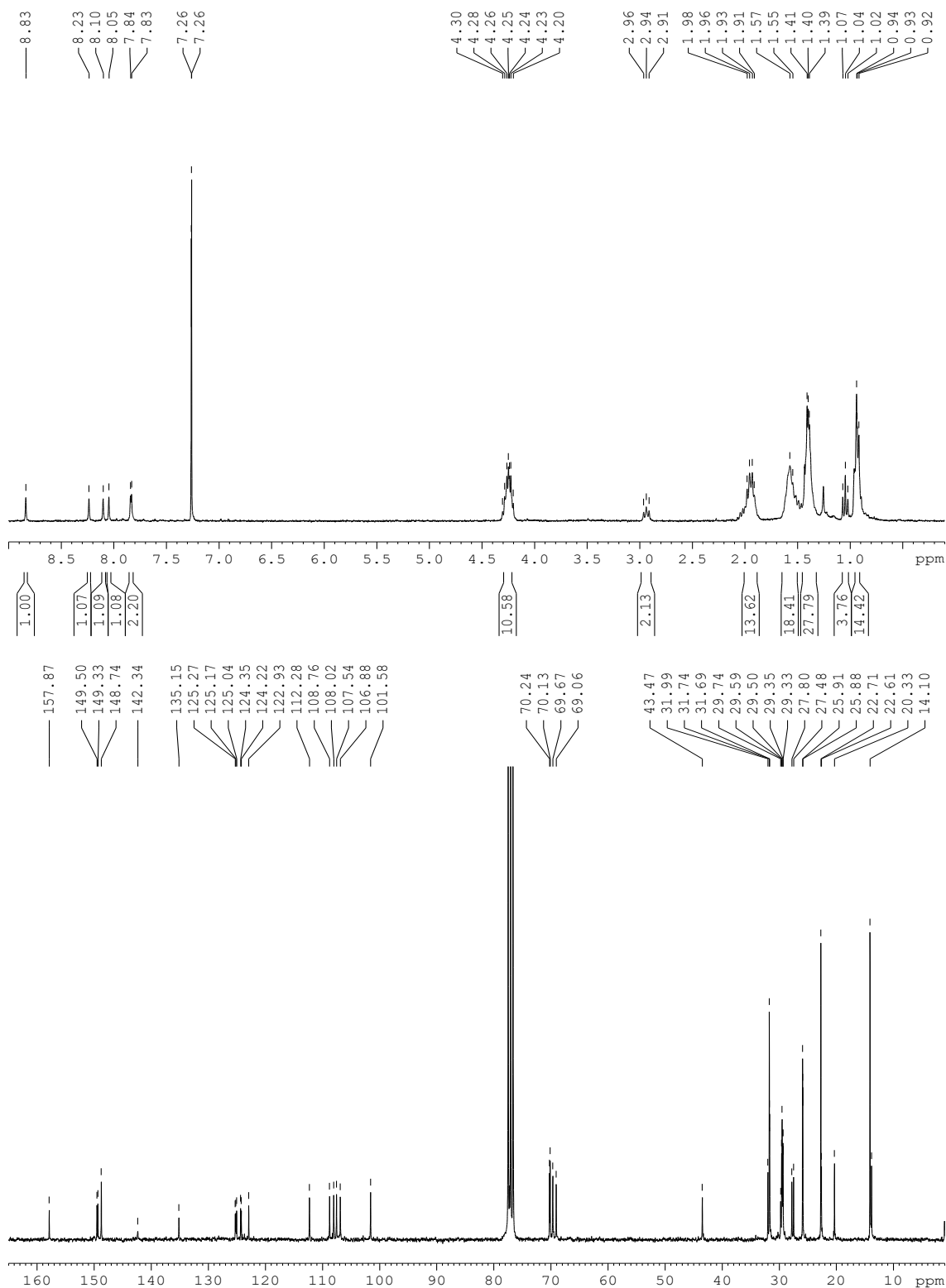
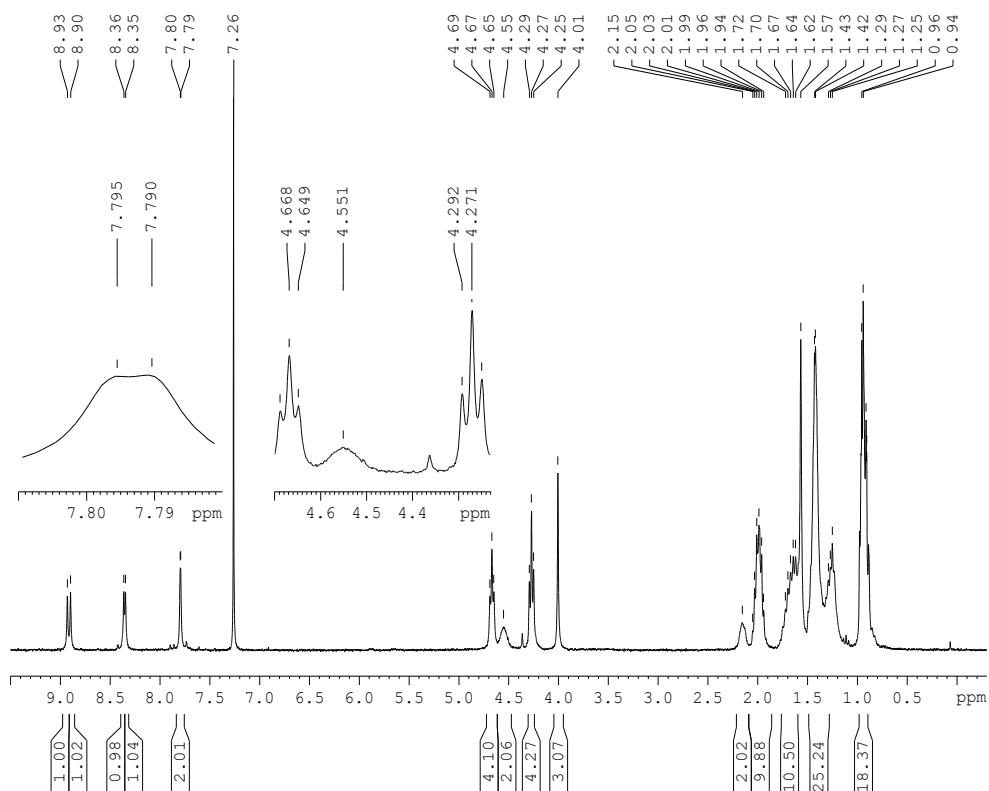


Figure S13. ¹H-NMR (up) and ¹³C-NMR (down) of **8-6** in CDCl₃

Synthesis of 10-butyl-11-hexyl-2,3,6,7-tetrakis(hexyloxy)-12-methyl-10H-triphenyleno[2,3-d]imidazol-12-ium iodide (9-6-I): The procedure is identical to the synthesis of **9-12-I** and yielded the product as a yellow solid in 85%.

$^1\text{H-NMR}$ (300 Hz, CDCl_3): δ (ppm) 8.93 (s, 1H, H_{Ar}), 8.90 (s, 1H, H_{Ar}), 8.36 (s, 1H, H_{Ar}), 8.34 (s, 1H, H_{Ar}), 7.79 (s_{broad} , two overlapping singlets, 2H, H_{Ar}), 4.67 (t, $J = 6.0$ Hz, two overlapping triplets, 4H, OCH_2), 4.55 (s_{broad} , 2H, NCH_2), 4.27 (t, $J = 6.0$ Hz, two overlapping triplets, 4H, OCH_2), 4.01 (s, 3H, NCH_3), 2.15 (s_{broad} , 2H, CH_2 , imine), 2.01-1.96 (m, 10H, CH_2), 1.64-1.56 (m, 10H, CH_2), 1.42-1.25 (m, 24H, CH_2), 0.98-0.91 (m, 18H, CH_3). $^{13}\text{C-NMR}$ (300 Hz, CDCl_3): δ (ppm) 152.88 (N-C=N), 150.64 (H_{Ar}), 150.19 (H_{Ar}), 150.08 (H_{Ar}), 129.73 (H_{Ar}), 129.10 (H_{Ar}), 127.99 (H_{Ar}), 123.95 (H_{Ar}), 123.84 (H_{Ar}), 122.52 (H_{Ar}), 108.53 (H_{Ar}), 108.28 (H_{Ar}), 107.28 (H_{Ar}), 107.07 (H_{Ar}), 106.73 (H_{Ar}), 106.59 (H_{Ar}), 71.42 (OCH_2), 70.00 (OCH_2), 46.59 (NCH_2), 34.44 (CH_2), 32.03 (CH_2), 31.84 (CH_2), 30.95 (CH_2), 29.55 (CH_2), 29.22 (CH_2), 26.84 (CH_2), 26.21 (CH_2), 26.00 (CH_2), 23.69 (CH_2), 22.80 (CH_2), 22.46 (CH_2), 20.04 (CH_2), 14.24 (CH_3), 14.19 (CH_3), 14.06 (CH_3), 13.84 (CH_3). IR (KBr) ν_{max} (cm^{-1}): 2954, 2927, 2857, 1611, 1514, 1454, 1432. HRMS ToF MALDI $^+$ m/e for $\text{C}_{54}\text{H}_{83}\text{N}_2\text{O}_4$ calcd ($\text{M}^{++}\text{-I}^-$) calcd 823.6353, found 823.6318, and HRMS ToF MALDI $^-$ m/e for (I^-) calcd 126.9045, found 126.9049.



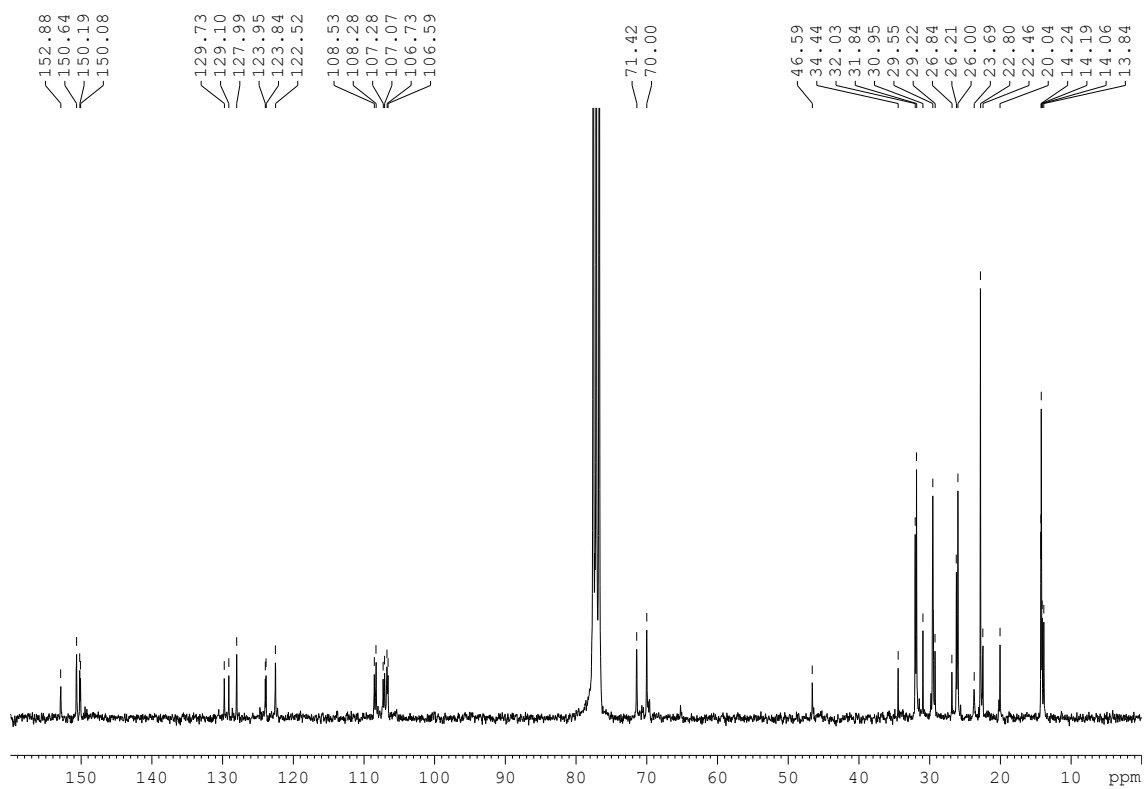


Figure S14. ^1H -NMR and ^{13}C -NMR of **9-6-I** in CDCl_3

Purity of compounds

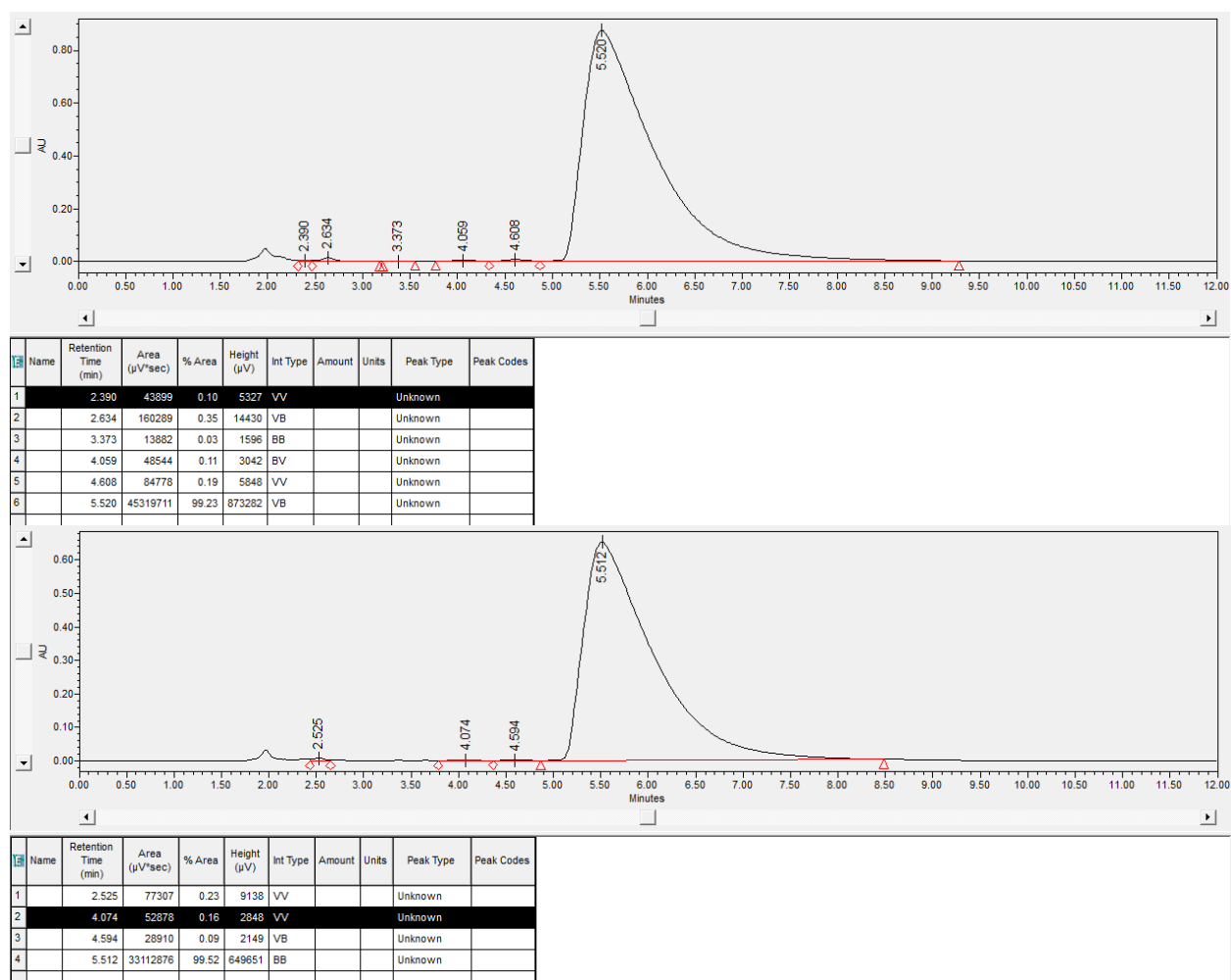
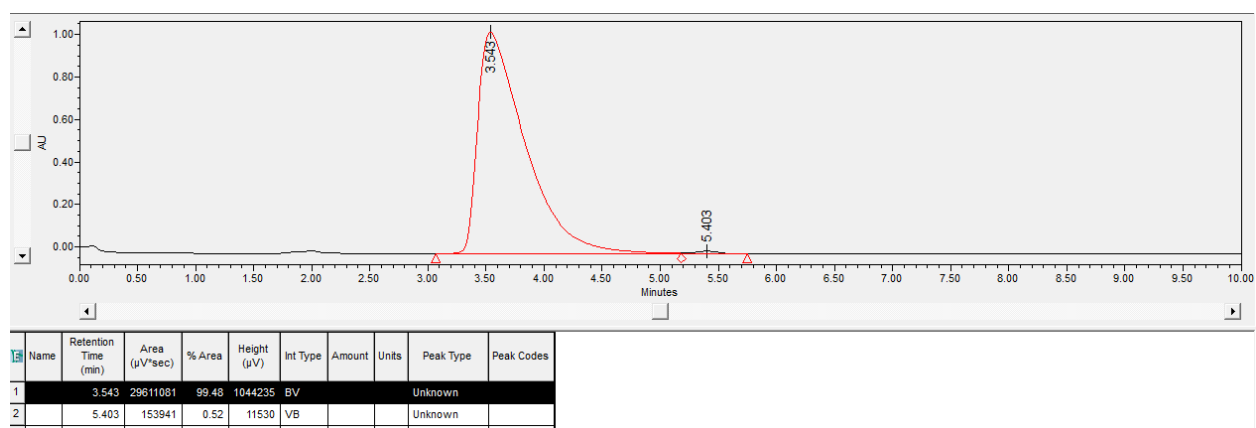


Figure S15. Chromatograms of compound **8-6** in 1,2-dichloroethane monitored at 260 nm (top) and 310 nm (bottom). Integration gives an HPLC purity of >99%. The minimum retention time is 1.95-2.00 min.



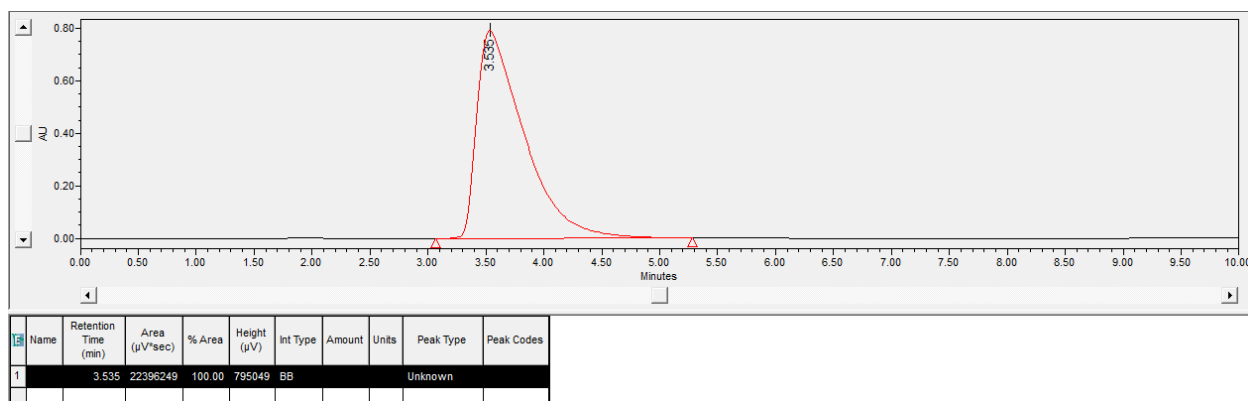


Figure S16. Chromatographs of compound **8-12** in 1,2-dichloroethane monitored at 260 nm (top) and 310 nm (bottom). Integration gives an HPLC purity of >99%. The minimum retention time is 1.95-2.00 min

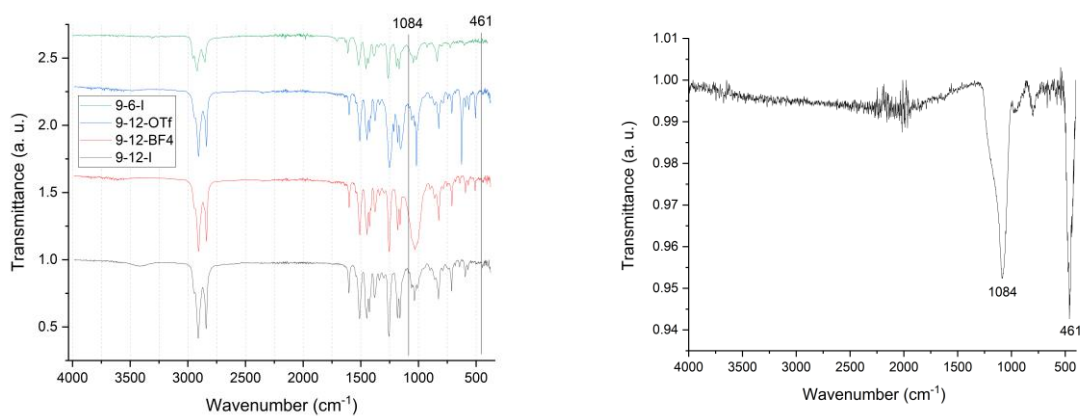


Figure S17. FT-IR spectra (ATR) of imidazolium compounds **9-n-x** (left) and silica gel 60 (35-70 mesh ASTM, from EM Science) used for chromatography (right). The two intense absorptions of silica gel are not seen in the IR spectra of compounds **9-n-x**.

Mesomorphism

Polarized light microscopy was performed on an Olympus TPM51 polarized light microscope that is equipped with a Linkam variable temperature stage HCS410 and digital photographic imaging system (DITO1). Calorimetric studies were conducted on a Mettler Toledo DSC 822^e and thermal gravimetric analysis was performed on a Mettler Toledo TGA SDTA 851e. Helium (99.99%) was used to purge the system at a flow rate of 60 mL/min. Samples were held at 30 °C for 30 min before heated to 550 °C at a rate of 5 °C/min. All samples were run in aluminum crucibles. XRD measurements were conducted on a Bruker D8 Discover diffractometer equipped with a Hi-Star area detector and GADDS software package. The tube is operated at 40 kV and 40 mA and CuK α 1 radiation (1.54187 Å) with an initial beam diameter of 0.5 mm is used. A modified Instec hot & cold stage HCS 402 operated via controllers STC 200 and LN2-P (for below ambient temperatures) was used for variable temperature XRD measurements. All samples were purified by filtering their solutions in dichloromethane through syringe filters with a pore diameter of 0.2 μ m to remove any particulate such as silica.

Polarized Optical Microscopy (POM)

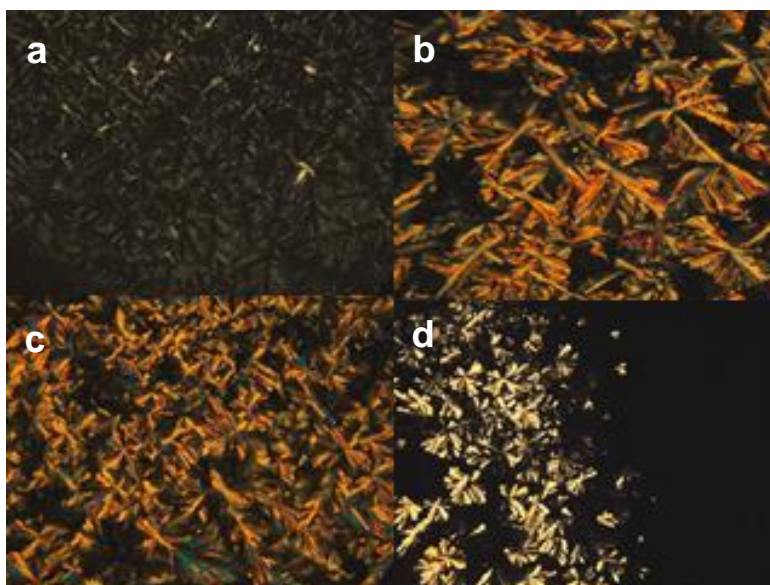


Figure S18. Photomicrographs (crossed polarizers, 100x magnification) of samples sandwiched between two glass slides upon cooling from their isotropic phases at 2 °C/min. (a) Col_h phase of **9-12-I** at 194 °C, (b) Col_h phase of **9-12-BF₄** at 110 °C, (c) Col_h phase of **9-12-OTf** at 147 °C, (d) Col_h phase of **9-6-I** at 145 °C on heating. The fan-shaped and dendritic defect textures with pseudo-isotropic areas of homeotropically aligned domains are characteristic for hexagonal columnar mesophases.

Thermal Gravimetric Analysis (TGA)

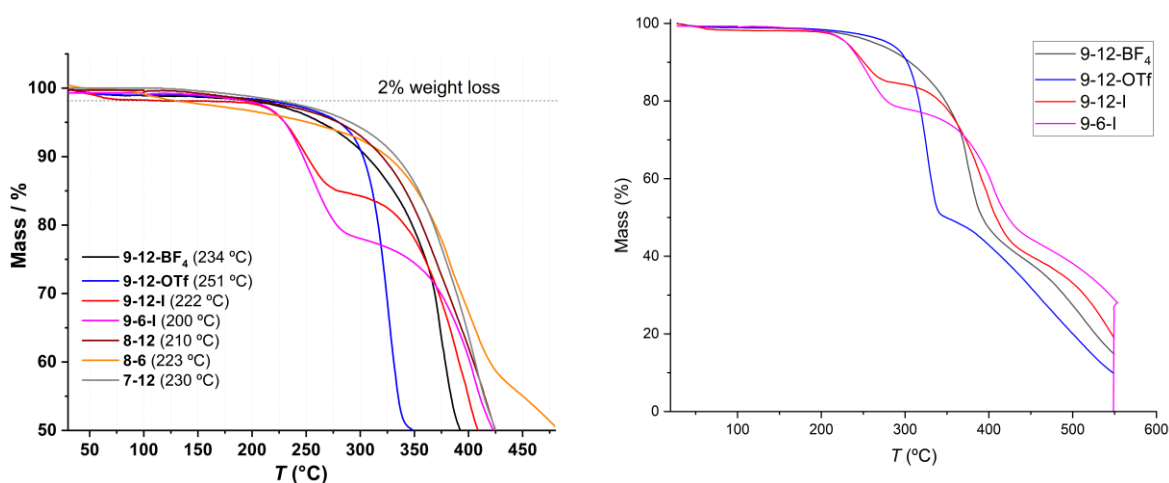


Figure S19. TGA graphs of compounds **7-12**, **8-n**, and **9-n-X** at 2 °C/min under He, except for **9-6-I** that was run at 10 °C/min. All samples were dried in vacuum at room temperature prior to TGA measurements but residual solvent was detected for **8-6** (2.0% by weight between 80 °C - 130 °C), **9-12-I** (1.8 wt% between 30 °C - 70 °C), **9-12-BF₄** (1.0 wt% between 30 °C - 80 °C), and **9-12-OTf** (1.0 wt% between 30 °C - 80 °C). The temperature at which a weight loss of 2% has occurred, excluding losses of solvent below 100 °C, were taken as an estimation of thermal stability and are provided in brackets in the legend. The isothermal segments at the beginning (10 min) remove any volatile compounds and the isothermal segment (550 °C for 1-2 hrs) at the end of each run completes the decomposition process. All samples **9-n-x** reach values below 3 wt% of residual mass.

Differential Scanning Calorimetry (DSC)

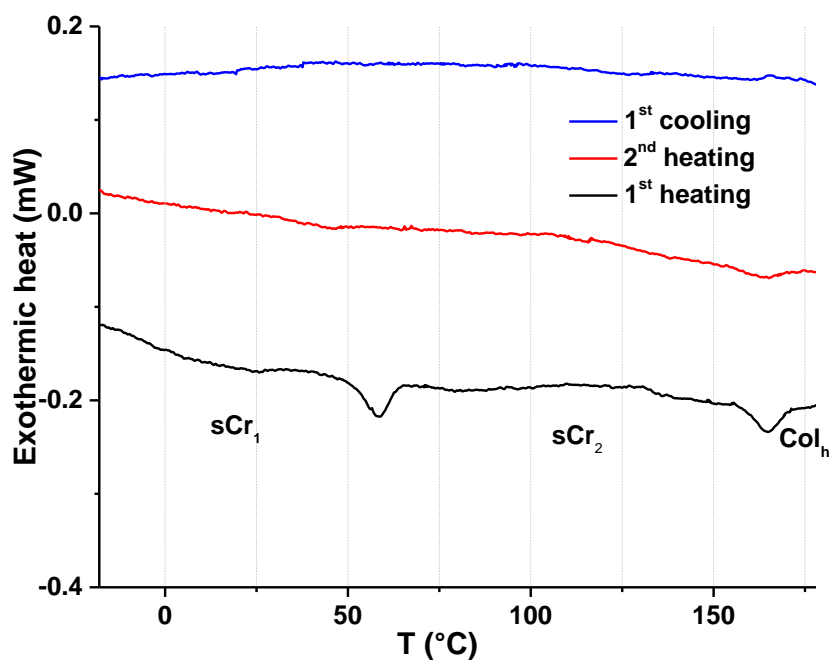


Figure S20. DSC graphs (baseline corrected) of **9-6-I** at 5 °C/min under N_2 . The crystal-crystal and melting transitions at 51 °C and 158 °C are well resolved in the first heating run but are weaker and broader in the subsequent heating runs because the sample crystallizes very slowly. This also explains the absence of peaks in the cooling runs. The clearing transition (Col_h to isotropic liquid) observed by POM at 216 °C was not detected by DSC because its transition enthalpy is likely small and the transition coincides with decomposition.

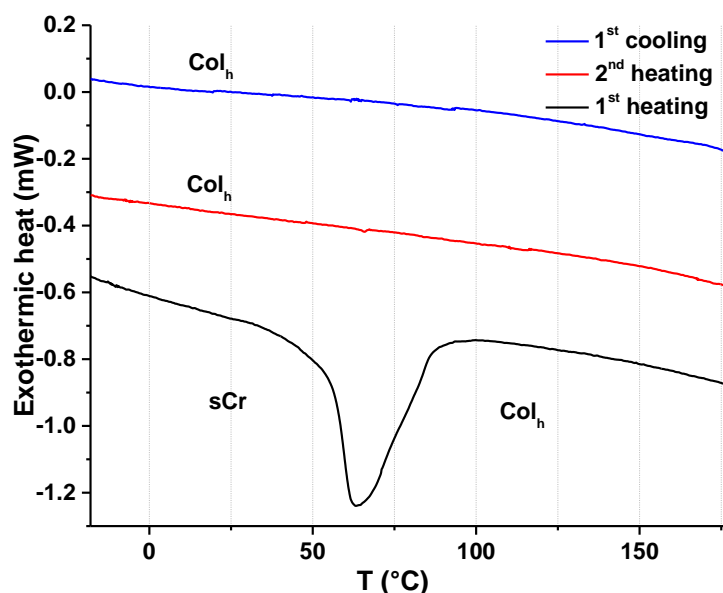


Figure S21. DSC graphs (baseline corrected) of **9-12-I** at 5 °C/min under N_2 . The melting transition at 54 °C is observed only in the first heating run as crystallization is kinetically hindered at this cooling rate. Crystallization occurred when the compound was kept at room temperature for 14 hrs. The clearing transition (Col_h to isotropic liquid) observed by POM at 209 °C was not detected by DSC because it has a too low transition enthalpy and/or is too broad.

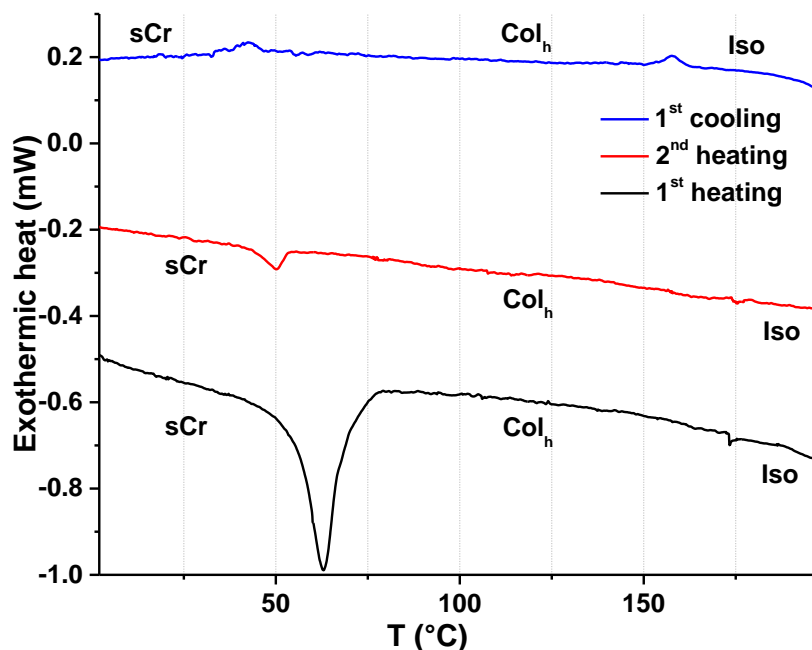


Figure S22. DSC graphs (baseline corrected) of **9-12-BF₄** at 5 °C/min under N₂. The melting and clearing transitions at 57 °C and 173 °C, respectively, are observed in all heating and cooling runs but only partial crystallization occurs at this cooling rate.

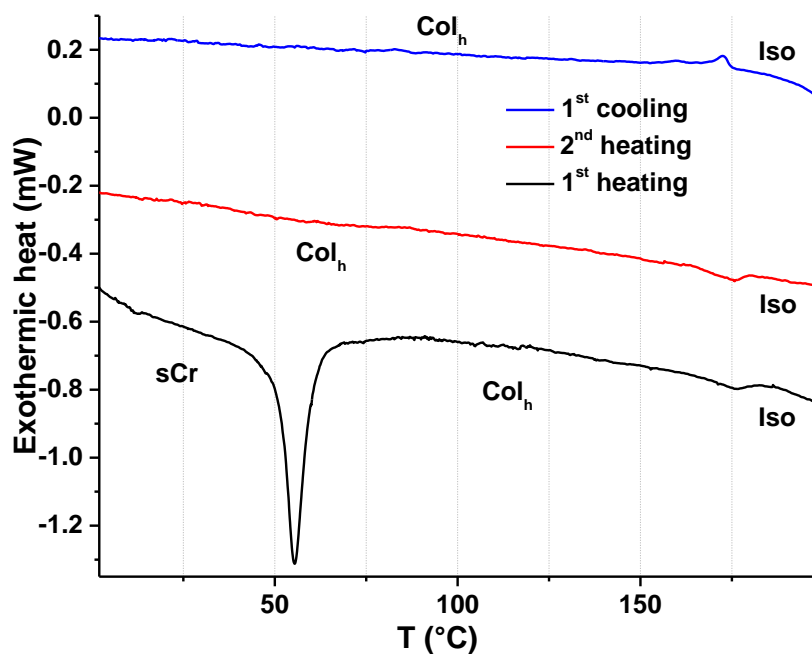


Figure S23. DSC graphs (baseline corrected) of **9-12-OTf** at 5 °C/min under N₂. Crystallization occurred when the compound was kept at room temperature for 14 hrs. The onset temperatures of the clearing transitions (Col_h to Iso) are below the onset temperature of the formation of the Col_h phase on cooling because the clearing transitions are unusually broad. Peak temperatures are at 176 °C and 173 °C for the clearing and Iso to Col_h transitions, respectively.

Variable Temperature Powder X-ray Diffraction (vt-pXRD)

All samples were run as circular pellets situated in a 1 mm thick copper plate with a central hole of 1 mL diameter. Sufficiently viscous liquids remain in the hole after melting due to capillary forces unless they come in contact with other objects.

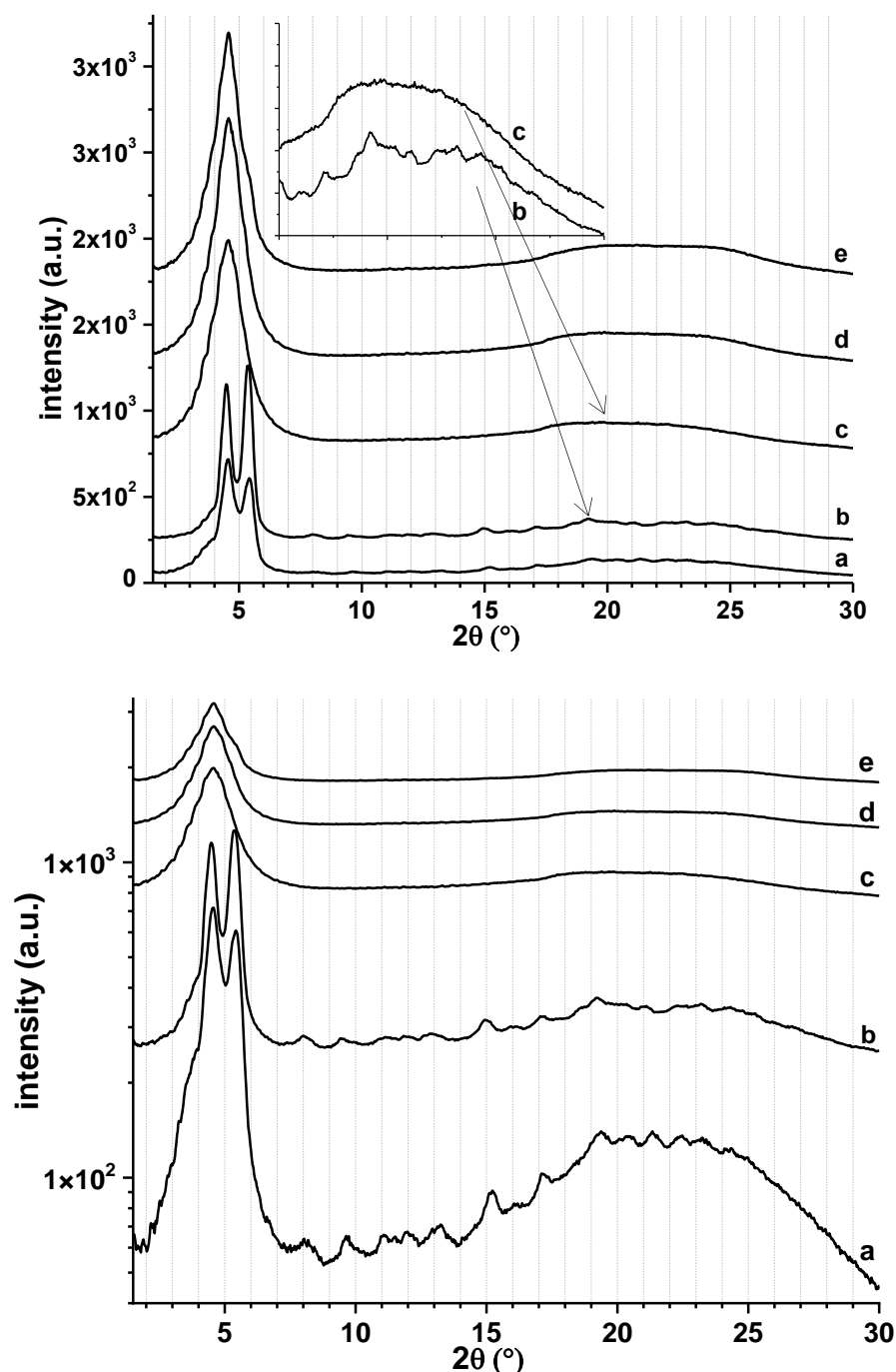


Figure S24. Diffraction patterns of **9-6-I**. (a) 25 °C, soft crystal phase (sCr1) obtained by precipitation from solution; (b) 65 °C, first heating, second soft crystal phase (sCr2); (c) 170 °C, first heating, Col_h; (d) 90 °C, on cooling from 170 °C, Col_h; (e) 25 °C, on cooling from 90 °C, Col_h. The compound converted to the soft crystal phase sCr1 after several hours at 25 °C. Multiple reflections between 19°–23° 2θ in patterns (a) and (b) are indicative of (partially) crystalline alkyl chains and their absence in patterns (c) – (e) is consistent with the presence

of a liquid crystal phase. Patterns (c) – (e) contain only one intense reflection in the small angle range that is assigned to the (10) reflection of a Col_h mesophase and two broad reflections at 20° and $25^\circ 2\theta$ that are characteristic for the halo of amorphous aliphatic chains and the π - π stacking reflection, respectively. In the absence of a characteristic (11) reflection, the liquid crystal phase assignment as Col_h is confirmed by its characteristic dendritic defect texture, which excludes smectic mesomorphism, and its pseudo-isotropic appearance when homeotropically aligned, which excludes the presence of optically biaxial columnar mesophases. The bottom graph has a logarithmic scale that helps with viewing small peaks of the bottom diffraction patterns but visually shrinks the intensity of the top diffraction patterns when stacked. No attempt was made to adjust this.

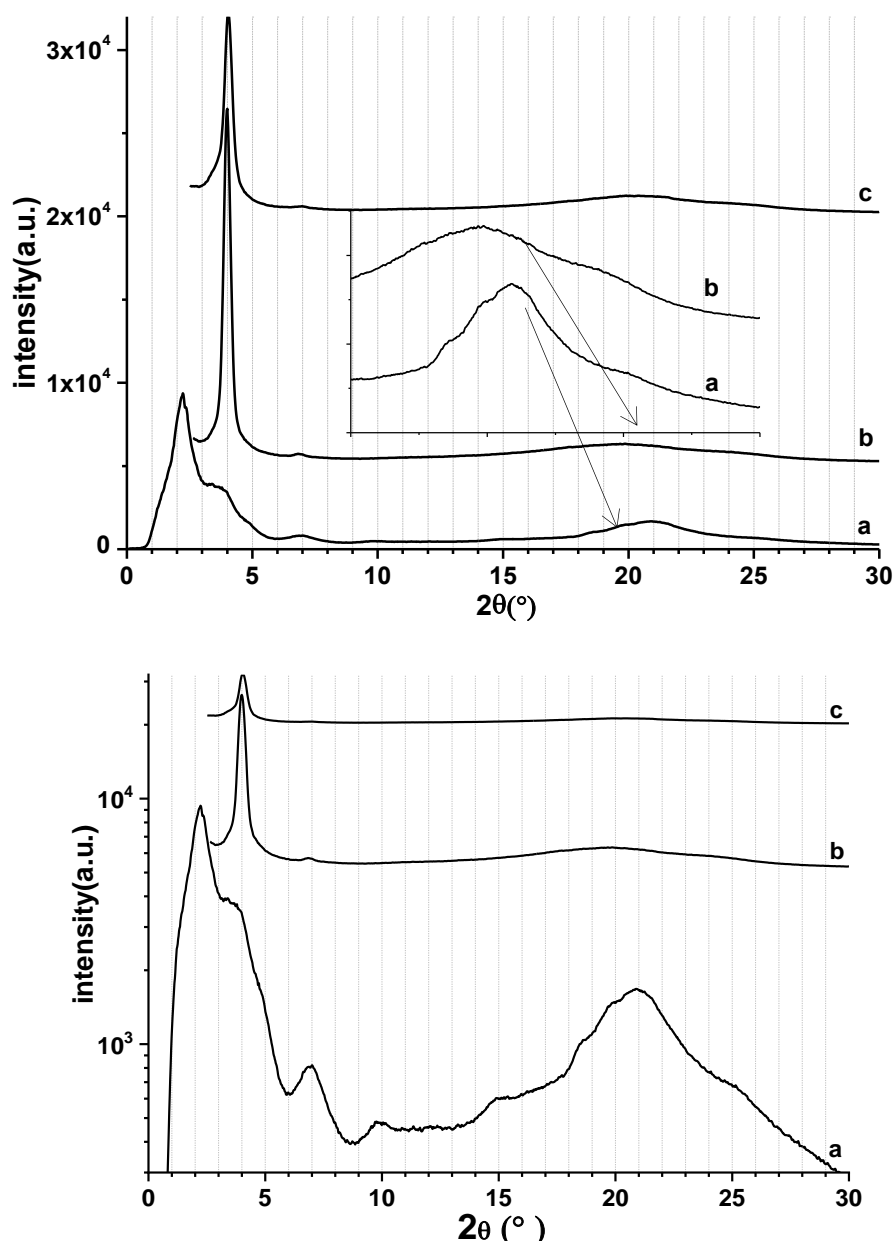


Figure S25. Diffraction patterns of **9-12-I**. (a) 20°C , soft crystal phase obtained by precipitation from solution; (b) 65°C , first heating, Col_h ; (c) 25°C , on cooling, Col_h . The compound solidified to the original soft crystal phase after 14 hrs at 25°C . The bottom graph has a logarithmic scale that helps with viewing small peaks of the bottom diffraction patterns but visually shrinks the intensity of the top diffraction patterns when stacked. No attempt was made to adjust this.

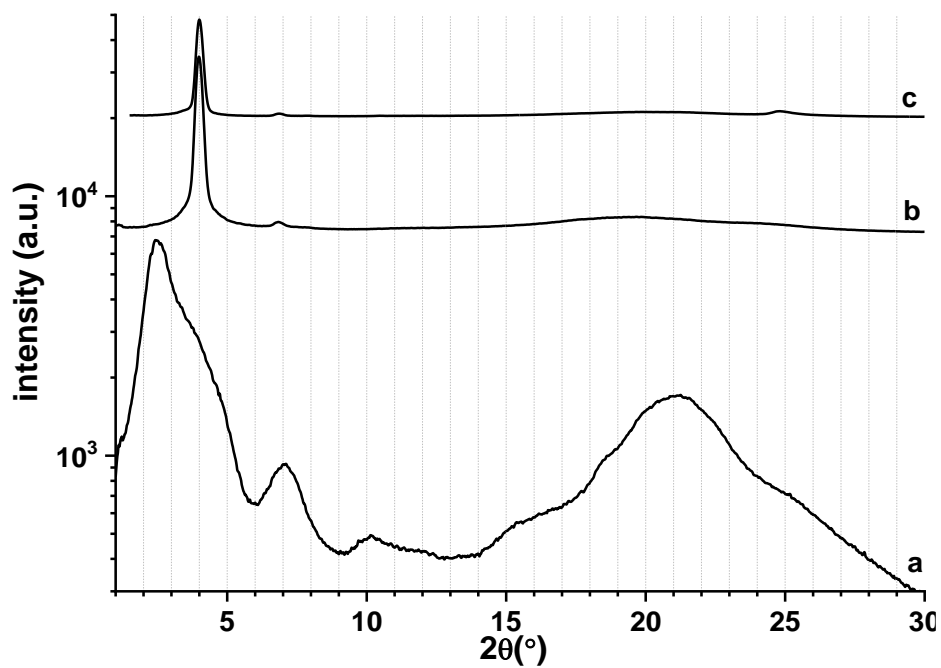
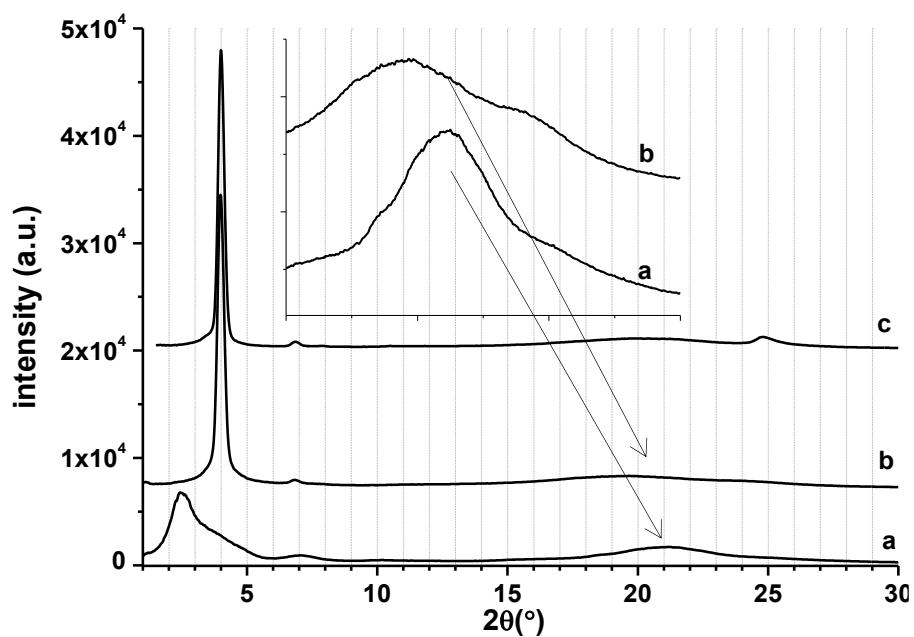


Figure S26. Diffraction patterns of **9-12-BF₄**. (a) 20 °C, soft crystal phase obtained by precipitation from solution; (b) 65 °C, first heating, Col_h; (c) 25 °C, on cooling from the isotropic liquid, Col_h. At 25 °C, the compound remains in the Col_h phase for several weeks. The bottom graph has a logarithmic scale that helps with viewing small peaks of the bottom diffraction patterns but visually shrinks the intensity of the top diffraction patterns when stacked. No attempt was made to adjust this.

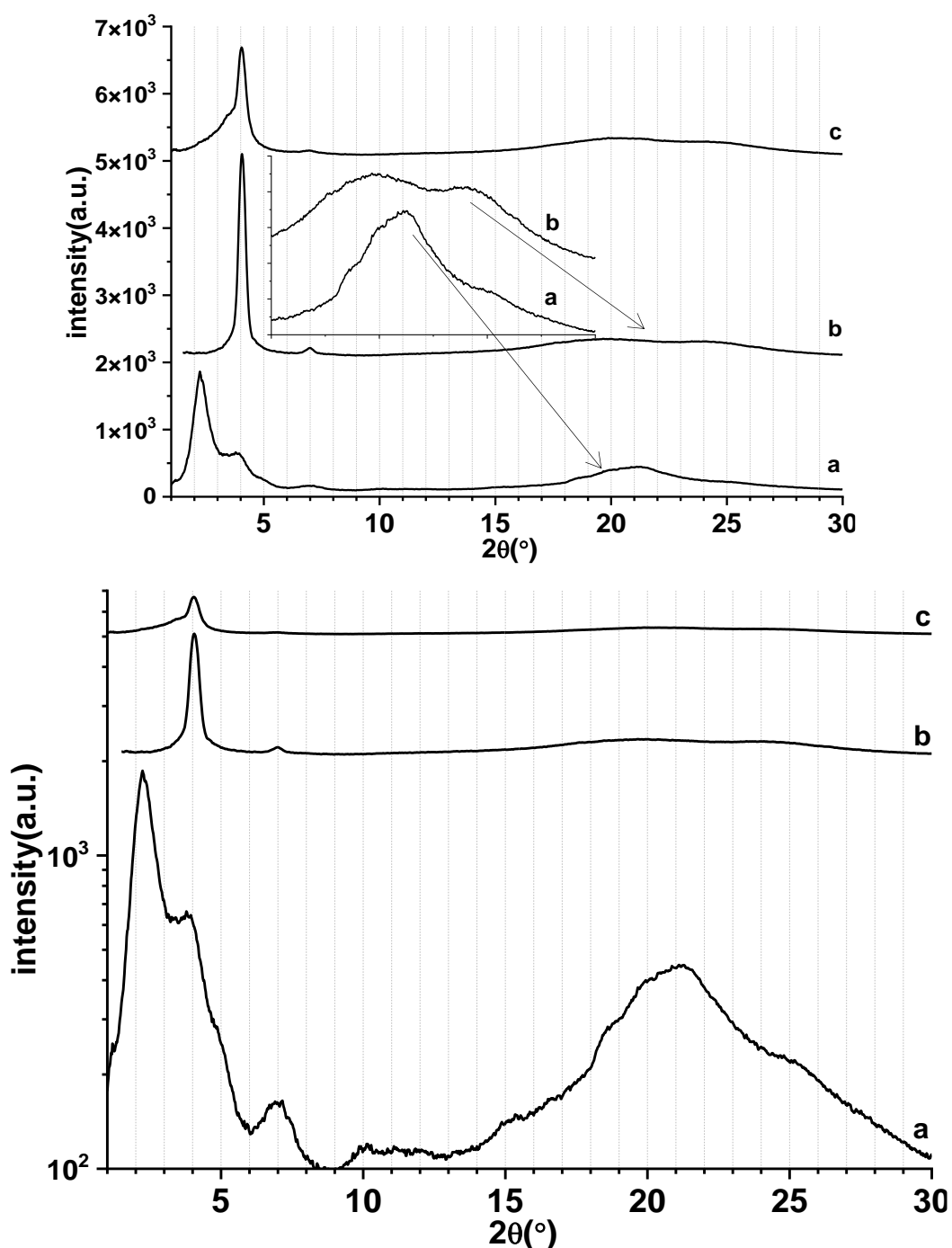


Figure S27. Diffraction patterns of 9-12-OTf. (a) 20 °C, soft crystal phase obtained by precipitation from solution; (b) 65 °C, first heating, Col_h; (c) 25 °C on cooling from the isotropic liquid. At 25 °C, the compound remains in the Col_h phase for several weeks although a splitting of the (10) reflection (shoulder to smaller angles) appears right away in the diffraction pattern. The bottom graph has a logarithmic scale that helps with viewing small peaks of the bottom diffraction patterns but visually shrinks the intensity of the top diffraction patterns when stacked. No attempt was made to adjust this.

Table S1. Detailed indexation of the hexagonal columnar mesophases of compounds **9-6-I**, **9-12-I**, **9-12-BF₄**, and **9-12-OTf** at the given temperature on heating. 2θ is the diffraction angle (in degrees). d_{obs} and d_{calc} are the corresponding observed and calculated d -spacings (in Å), respectively. I is the relative intensity of a diffraction peak. hk is the indexation of the two-dimensional lattice. a is the lattice parameter, S_h is the calculated area of the cross section of a columnar stack based on the hexagonal lattice parameter a . V_h is the calculated volume of an individual discotic unit (section of the column) based on S_h and the π - π stacking distance h_{stack} of the periodic stacking of discotic units. V_{mol} is the calculated molecular volume as described in the next section.

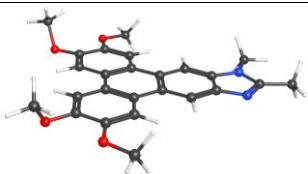
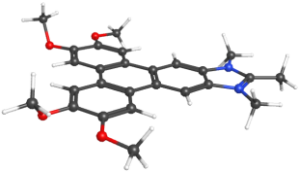
9-6-I						
T (°C)	2θ (°)	d_{obs} (Å)	I	hk (p6mm)	d_{calc} (Å)	Col _h , p6mm $a = 22.2 \text{ \AA}$ $S_h = 426 \text{ \AA}^2$ $V_h = 1610 \text{ \AA}^3$ (for 3.78 Å) $V_h = 1534 \text{ \AA}^3$ (for 3.6 Å) $V_{mol} = 1508 \text{ \AA}^3$
90	4.6	19.2	100	10	19.2	
	19.9 ^a	4.5	17.5	halo _{alkyl}		
	23.5	3.8 ^b	16.5	h_{stack}		
9-12-I						
T (°C)	2θ (°)	d_{obs} (Å)	I	hk (p6mm)	d_{calc} (Å)	Col _h , p6mm $a = 25.1 \text{ \AA}$ $S_h = 549 \text{ \AA}^2$ $V_h = 2081 \text{ \AA}^3$ (for 3.79 Å) $V_h = 1976 \text{ \AA}^3$ (for 3.6 Å) $V_{mol} = 2150 \text{ \AA}^3$
65	4.06	21.8	100	10	21.8	
	7.00	12.6	8.5	11	12.6	
	19.7 ^a	4.5	11.5	halo _{alkyl}		
	23.5	3.8 ^b	10.3	h_{stack}		
9-12-BF₄						
T (°C)	2θ (°)	d_{obs} (Å)	I	hk (p6mm)	d_{calc} (Å)	Col _h , p6mm $a = 25.6 \text{ \AA}$ $S_h = 569 \text{ \AA}^2$ $V_h = 2174 \text{ \AA}^3$ (for 3.82 Å) $V_h = 2048 \text{ \AA}^3$ (for 3.6 Å) $V_h = 1992 \text{ \AA}^3$ (for 3.5 Å) $V_{mol} = 2176 \text{ \AA}^3$
65	3.98	22.2	100	10	22.2	
	6.83	12.9	3.5	11	12.8	
	7.77	11.4	2.2	20	11.1	
	19.7 ^a	4.5	4.9	halo _{alkyl}		
	23.3	3.8 ^b	3.4	h_{stack}		
9-12-OTf						
T (°C)	2θ (°)	d_{obs} (Å)	I	hk (p6mm)	d_{calc} (Å)	Col _h , p6mm $a = 25.5 \text{ \AA}$ $S_h = 564 \text{ \AA}^2$ $V_h = 2154 \text{ \AA}^3$ (for 3.82 Å) $V_h = 2030 \text{ \AA}^3$ (for 3.6 Å) $V_{mol} = 2223 \text{ \AA}^3$
65	4.00	22.1	100	10	22.1	
	6.84	12.9	3.6	11	12.8	
	19.7 ^a	4.5	6.4	halo _{alkyl}		
	23.3	3.8 ^b	4.3	h_{stack}		

^aDiffuse broad reflection (halo) of aliphatic side-chains in an amorphous (molten) state; ^bStacking distance in the columnar arrangement.

Equations used for calculations of a , S_h and V_h : $a = \sqrt{\frac{4}{3}}d_{10}$, $S = S_h = \frac{2}{\sqrt{3}}d_{10}^2$, $V_h = h_{stacking} * S_h$

Molecular volume calculations

Table S2. V_{mol} is calculated as the sum of the core volume (V_{core}) and the side-chain volume ($V_{\text{s-c}}$). The core and anion volumes were estimated by DFT calculations (6-31+G(d,p)) as IPCM solvent cavity in cyclohexane with two different functionals (B3LYP and ω B97X-D) for the compounds with methyl groups as alkyl chains. The values for ω B97X-D were used for the calculations of V_{mol} . Volumes of hydrocarbon chains have been measured at different temperatures and can be calculated based on the following empirical equation: V_{CH_2} (in \AA^3) = $26.5616 + 0.02023 T$ (T in $^\circ\text{C}$). Terminal methyl groups of linear alkyl groups are counted as methylene groups and the following value is added to adjust for the larger volume of a terminal methyl group: V_{CH_3} (in \AA^3) = $V_{\text{CH}_2} + 27.14 + 0.01713 T + 0.0004181 T^2$.³

	V_{core} B3LYP	V_{core} ω B97X-D**	$V_{\text{s-c}}$ ***
	510.7238 \AA^3	500.5869 \AA^3	8-6 at 90 $^\circ\text{C}$ 987.1142 \AA^3 8-12 = at 65 $^\circ\text{C}$ 1629.7001 \AA^3
	489.4802 \AA^3 + anion $\text{I}^- = 44.602 \text{\AA}^{3*}$ $\text{BF}_4^- = 72.2936 \text{\AA}^3$ $\text{CF}_3\text{SO}_3^- = 119.7206 \text{\AA}^3$	475.8514 \AA^3 + anion $\text{I}^- = 44.602 \text{\AA}^{3*}$ $\text{BF}_4^- = 70.92598 \text{\AA}^3$ $\text{CF}_3\text{SO}_3^- = 117.4727 \text{\AA}^3$	9-6-I (90 $^\circ\text{C}$) 987.1142 \AA^3 9-12-I (65 $^\circ\text{C}$) 1629.7001 \AA^3 9-12-BF₄ (65 $^\circ\text{C}$) 1629.7001 \AA^3 9-12-OTf (65 $^\circ\text{C}$) 1629.7001 \AA^3

*Volume of iodide based on estimated ionic radius of 2.20 \AA (<http://abulafia.mt.ic.ac.uk/shannon/ptable.php>; Hosted by the Atomistic Simulation Group in the Materials Department of Imperial College) because the used all-electron basis set is not parameterized for iodine. Reported estimated ionic radii for BF_4^- and OTf^- are 2.29 \AA and 2.70 \AA , which give spherical volumes of 50.30 \AA^3 and 82.45 \AA^3 .⁴ However, the larger volumes estimated by DFT calculations were used for BF_4^- and OTf^- . **Used for calculation of V_{mol} . ***One methylene group of each alkyl chain was omitted for the calculation of $V_{\text{s-c}}$ since a methyl group is already included in the core structure.

Computational Details and Data

All calculations were performed using the Gaussian16 suite of programs.⁷ The full study (monomers and stacks of five monomers) was carried out with the semi-empirical PM6;⁸ all geometries were fully optimized in the gas phase. To ensure that empirical dispersion does not impact the computed anion placement, monomeric (methyl-only) bromides were additionally optimized within density-functional theory (DFT), using Becke's 3-parameter exchange functional and the Lee-Yang-Parr correlation functional (B3LYP)⁹⁻¹¹ as well as Head-Gordon's long-range corrected hybrid functional with dispersion correction ω B97X-D,¹² both with the all-electron 6-31+G(d,p) basis set (the use of pseudo-potentials for iodide was avoided). To evaluate the dielectric environment of a monomer within a stack, selected monomeric salts were optimized in a solvent field, using the PCM (Polarizable Continuum Model)¹³ treatment as implemented in Gaussian 16, with cyclohexane (ϵ 2.0165), chloroform (ϵ 4.7113) and dichloromethane (ϵ 8.93) as the solvent. While the reported estimated dielectric constant for the related ionic liquid 1-methyl-3-octylimidazolium tetrafluoroborate is given with 7.5,¹⁴ we finally decided on chloroform as a suitable solvent; all observed changes upon an increase in ϵ to that of dichloromethane were small. Changes in geometry between the semiempirical and DFT methods were found to be inconsequential within the context of liquid crystals. Again within this context, frequency analyses (298 K, 1 atmosphere, harmonic oscillator approximation) within a model chemistry established all optimized geometries as being minima, and searches for global minima were not carried out. PM6 free energies were determined at 298 and 350 K (1 atmosphere) in the gas phase. All electronic and free energies are given in Tables S3 and S4 (monomers) and S5 (stacks of monomers).

To match the environment in a columnar stack, molecular volumes (Table S2) for the cations were determined as the analogue of the solute cavity size, with cyclohexane as the solvent and within the IPCM (Isodensity Polarizable Continuum Model)¹⁵ solvent field treatment.

For atomic charges, wavefunctions for the optimized (in the gas phase or in a solvent field) monomers were obtained using the DFT methods at the same model chemistries; those for the stacks were taken from HF/3-21G//PM6. This approach is justified because the topology of the electron density (the location of its maxima and saddle points) is robust with respect to the choice of model chemistry and since a numerical analysis was not part of this work. Molecular graphs (networks of bonding interactions) and atomic charges were determined within the

quantum theory of atoms in molecules (QTAIM)¹⁶ through the program AIMAll.¹⁷ Geometries, dipole moments and molecular orbitals are depicted from WebMO.¹⁸

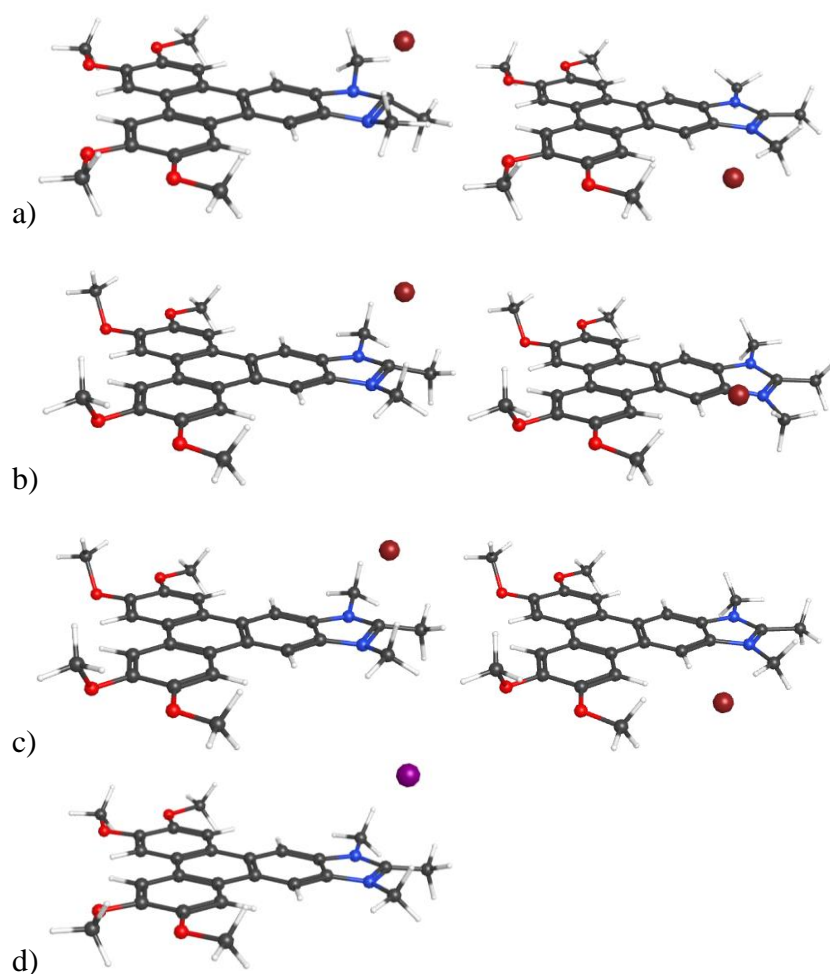


Figure S28. The two preferred positions of the bromide in the all-methyl ionic monomer (**9-1-Br**) in comparison (gas-phase geometries): on-top (left) and in the bay area (right). From a) PM6, b) B3LYP/6-31+G(d,p) and c) ω B97X-D/6-31+G(d,p). The PM6 on-top geometry in chloroform is shown in d) for the experimentally more relevant **9-1-I**.

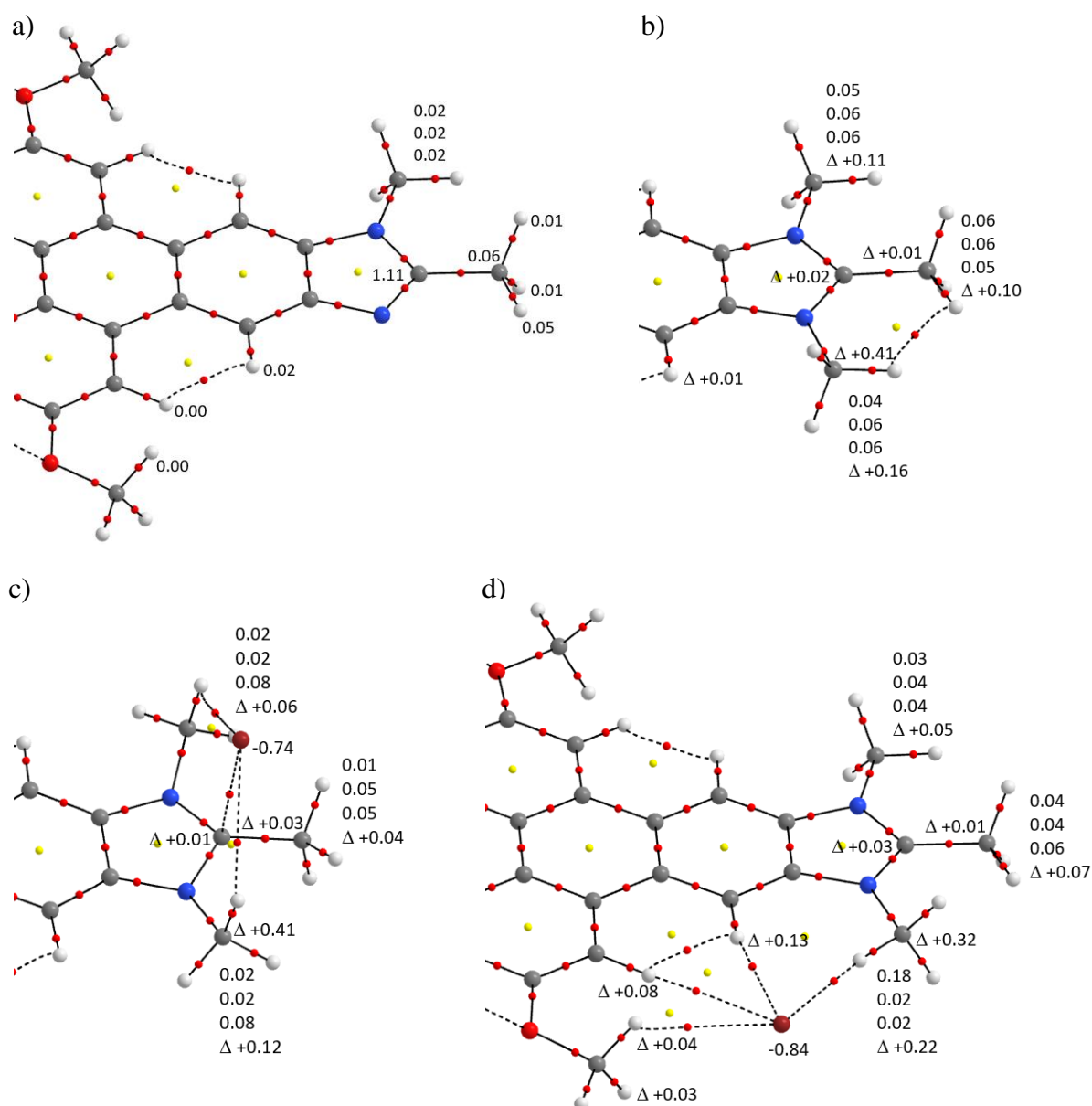


Figure S29. Selected atomic charges (from QTAIM, in au) in a) the uncharged parent **8-1**, and changes (Δ) in charge upon the introduction of the positive charge into the aromatic core b) without counterion (**9-1**) and c) to f) with bromide (**9-1-Br**), from ω B97X-D/6-31+G(d,p). **9-1-Br** charges are from gas phase geometries (c and d) and geometries in chloroform (e and f). Molecules are shown truncated.

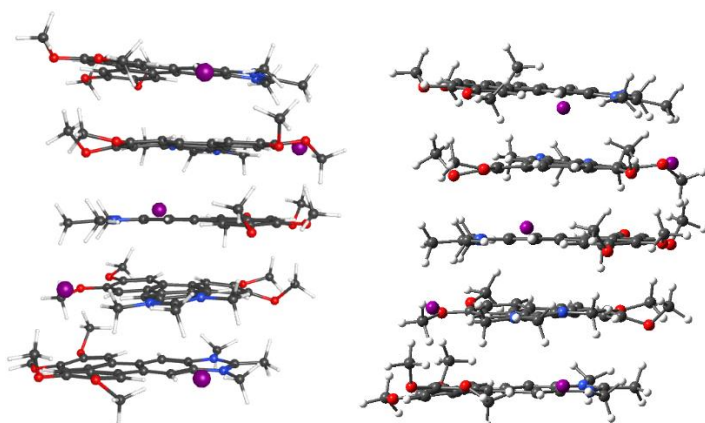


Figure S30. Views of the PM6-optimized all-methyl iodide 5-stack (**5-9-1I**), with (from WebMO, left) and without (from GaussView,¹⁹ right) perspective. The coplanarity of the monomers in the stack is visually emphasized in GaussView.

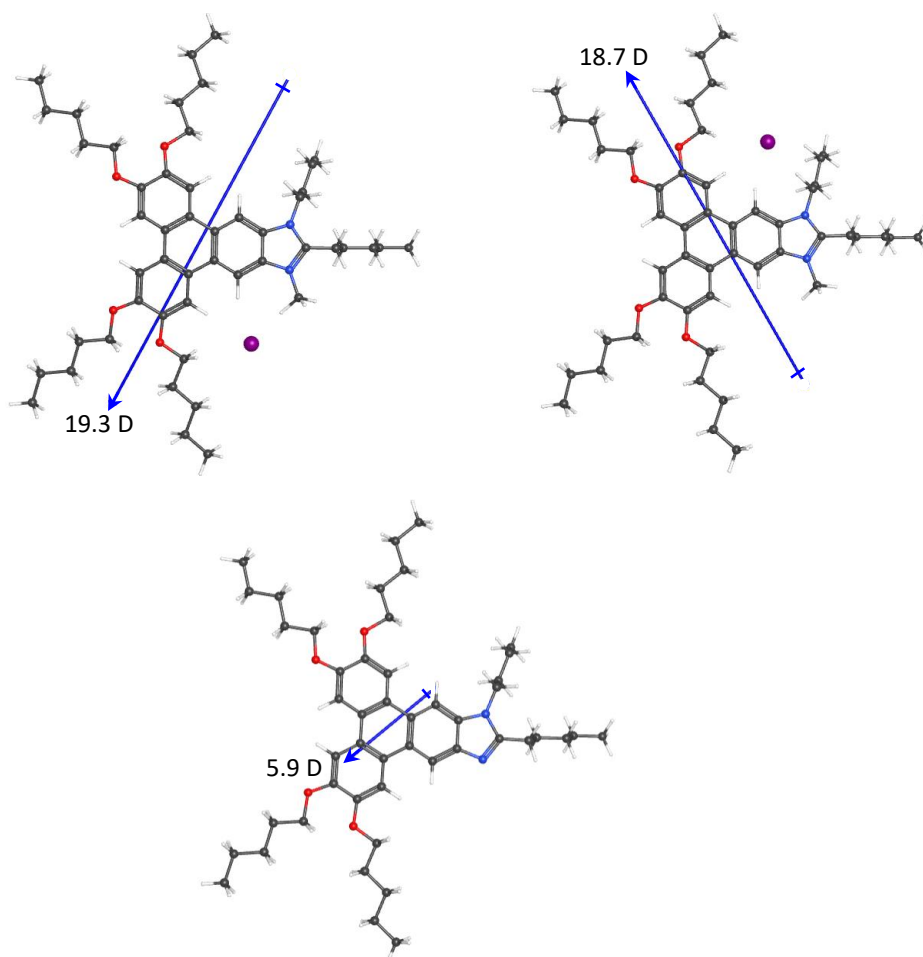

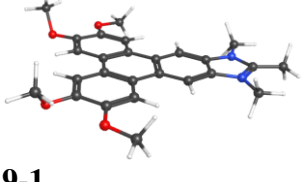
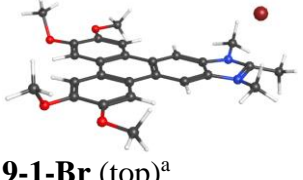
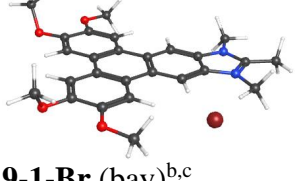
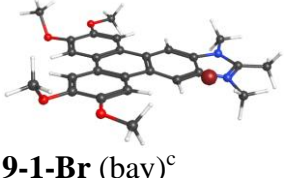


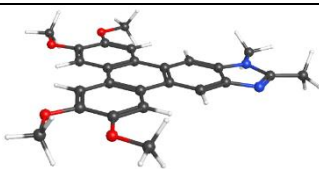
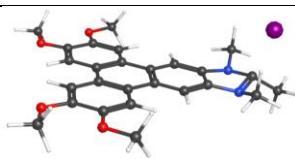
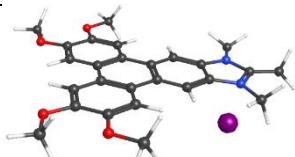
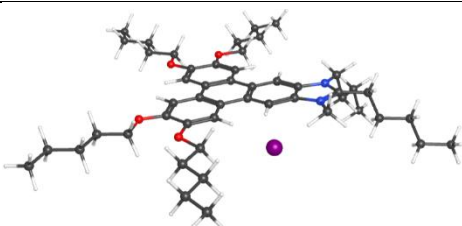
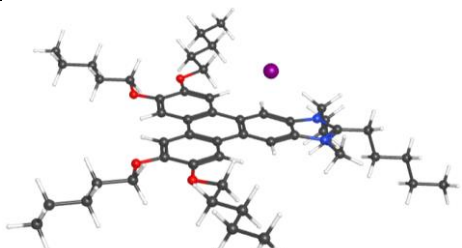
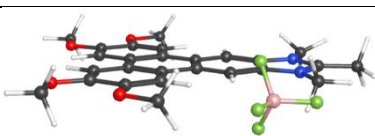
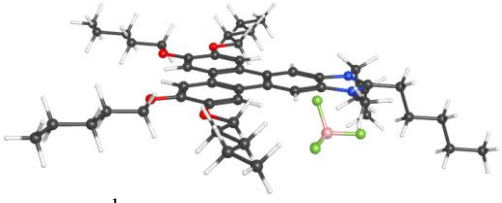
Figure S31. View of the dipoles and dipole moment of two **9-5-I** monomers, from PM6; **8-5** (bottom) given for comparison. Arrowheads were enhanced for visibility.

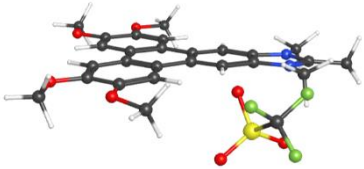
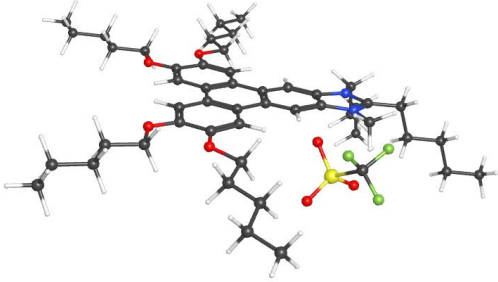
Table S3. Monomers **8-1**, **9-1** and **9-1-Br**: electronic (E_{el}) energy and free (G) energy (in Hartrees) at 298 K, from two DFT theories with the 6-31+G(d,p) basis set. Values in parentheses from optimizations in chloroform.

	ω B97X-D		B3LYP	
	E_{el}	G	E_{el}	G
 8-1	-1377.135356	-1376.746284	-1377.585124	-1377.202713
 9-1	-1416.836577	-1416.410111	-1417.295072	-1416.875787
 9-1-Br (top)^a	-3988.813334	-3988.387335	-3989.244995	-3988.825991
 9-1-Br (bay)^{b,c}	-3988.795813	-3988.371928		
 9-1-Br (bay)^c			-3989.227651	-3988.810806

^a Bromide position “on-top”. A second configuration with the bromide below the plane differs slightly in energies: ω B97X-D $\Delta E_{el} +0.26$, $\Delta G -0.10$; B3LYP $\Delta E_{el} +0.18$, $\Delta G +0.29$ kcal/mol. ^b Bromide in “bay” position. “Bay” here is chosen descriptively, not based on the notations of bay, fjord or cove as established for interactions to hydrogen atoms on sp^2 -hybridized carbon atoms in polycyclic aromatic hydrocarbons.¹⁸ ^c The bromide position in the bay differs slightly upon a change in DFT method: in-plane from ω B97X-D, out-of-plane by 1.9 Å from B3LYP.

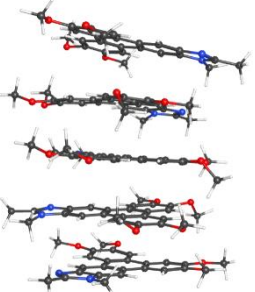
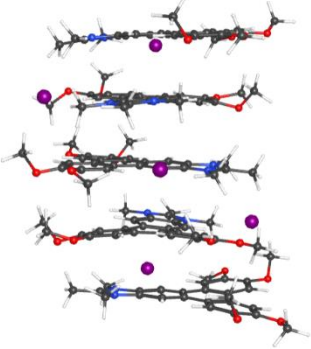
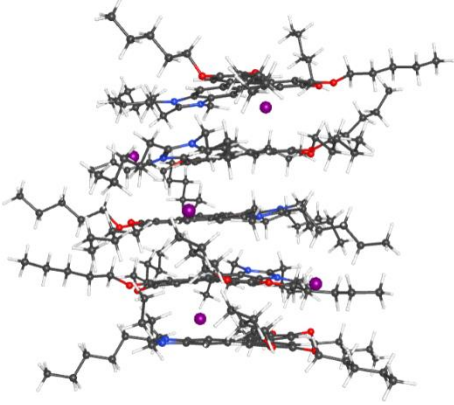
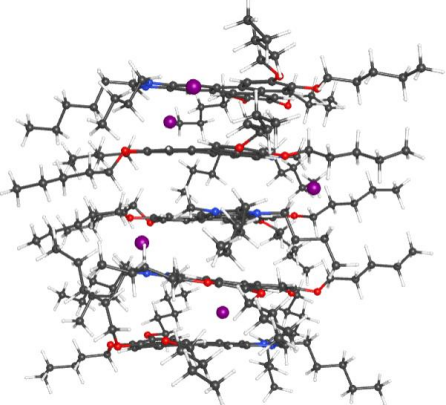
Table S4. Monomers: electronic (E_{el}) energy and free (G) energies (in Hartrees) at two temperatures, from PM6. Values in parentheses from optimization in chloroform; values in square brackets from gas phase energy evaluation of the chloroform-optimized geometry.

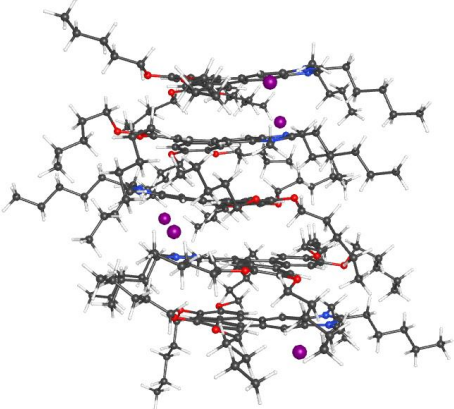
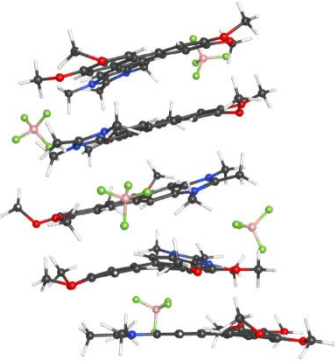
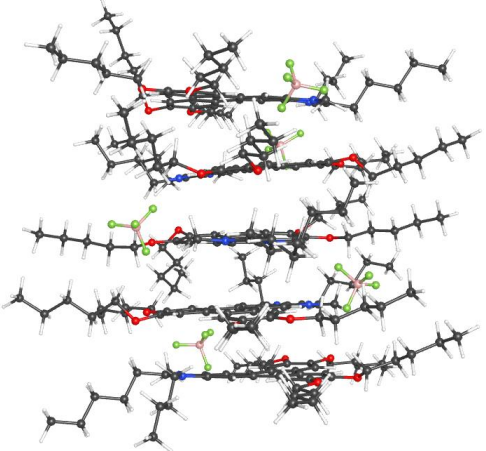
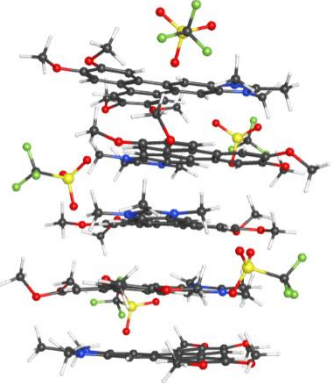
	E_{el}	G
 8-1^a	-0.103739	298 K: 0.239121 350 K: 0.221592
 9-1-I	-0.108112 ^b (-0.131916)	298 K: 0.265658 H 350 K ^c
 9-1-I	-0.097048 ^b (-0.135837) [-0.092998]	298 K: 0.271341 350 K: 0.251690
 9-5-I^d	-0.299332 (-0.335691) [-0.295567]	298 K: 0.616363 350 K: 0.580367
 9-5-I^d	-0.299272 (-0.335296) [-0.295864]	298 K: 0.616442 350 K: 0.580436
 9-1-BF₄	-0.681843 (-0.725394) [-0.678620]	298 K: -0.301024 350 K: -0.322326
 9-5-BF₄^d	-0.882892 (-0.923965) [-0.879456]	298 K: 0.043765 350 K: 0.005880

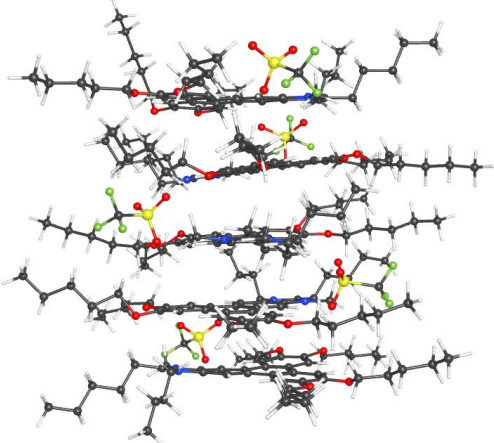
 <p>9-1-OTf</p>	<p>-0.553676 (-0.588480) [-0.551629]</p>	<p>298 K: -0.165744 350 K: -0.188269</p>
 <p>9-5-OTf^d</p>	<p>-0.755305 H (-0.787005) [-0.753423]</p>	<p>298 K: 0.180425 350 K: 0.141661</p>

^a For **8-1** with N-ethyl substitution: E_{el} -0.115949, G(298 K) 0.252271, G(350 K) 0.234314 H. ^b E_{el} for the optimized bromide: on-top -0.157822 H, in the bay -0.115823 H. ^c Not determined. ^d Anion in the N-methyl bay. ^e Iodide in the N-butyl bay.

Table S5. Stacks of five monomers: electronic (E_{el}) energy and free (G) energies (in Hartrees) at two temperatures, from PM6. For the **9-n-x** stacks, the bottom anion is shown in the back.

	E_{el}	G
 <p>8-1^a</p>	-0.576665	298 K: 1.245477 350 K: 1.175389
 <p>9-1-I^b</p>	-0.672904	298 K: 1.300433 350 K: 1.223759
 <p>9-5-I^b</p>	-1.692769	298 K: 3.073457 350 K: 2.925759
 <p>9-5-I^c</p>	-1.734373	298 K: 3.048948 350 K: 2.904441

 <p>9-5-I (alternating bays)^d</p>	-1.707102	298 K: 3.079224 350 K ^e
 <p>9-1-BF₄^b</p>	-3.577036	298 K: -1.559900 350 K: -1.648180
 <p>9-5-BF₄^b</p>	-4.615546	298 K: 0.206030 350 K: 0.049149
 <p>9-1-OTf^b</p>	-2.961092	298 K: -0.892545 350 K: -0.984000

 <p>9-5-OTf^b</p>	<p>-3.979129</p>	<p>298 K: 0.885136 350 K: 0.723249</p>
---	------------------	--

^a For the stack of five **8-1** with N-ethyl substituent: E_{el} -0.636285, $G(298\text{ K})$ 1.310026, $G(350\text{ K})$ 1.237371 H. ^b Anion in the N-methyl bay. ^c Iodide in the N-butyl bay. ^d Iodide alternating bays: three N-methyl, two N-butyl. ^e Not determined.

Table S6. Stabilization energy^a and free energy (kcal/mol) difference at two temperatures for stacks of five monomers; from PM6. Values in square brackets derived from the gas phase energy evaluation of the monomer geometry from its optimization in chloroform (see the bracketed values from Table S4).

	ΔE_{el}	ΔG (298 K)	ΔG (350 K)
8-1^b	-36.4	+31.3	+42.3
9-1-I	-117.8 [-130.5]	-35.3	-21.8
9-5-I^c	-123.1 ^d [-134.9]	-5.2	+15.0
9-5-1^e	-149.4 ^d [-160.0]	-20.9	+1.4
9-1-BF₄	-105.3 [-115.4]	-34.4	-22.9
9-5-BF₄^c	-126.2 [-137.0]	-8.0	+12.4
9-1-OTf	-120.9 [-123.7]	-40.1	-26.8
9-5-OTf^c	-127.1 [-133.0]	-10.7	+9.4

^a The stabilization energy [$E_{el}(\text{stack}) - 5 \cdot E_{el}(\text{monomer})$] is the negative of the binding energy.

ΔE_{el} was determined using a) the gas-phase energy of the bay-occupied monomer in its gas-phase geometry and b) in its geometry in a chloroform solvent field. ^b For the stack of five **8-1** with N-ethyl (torsion for the ethyl group approximately 90° to the imidazole plane) substituent: ΔE_{el} -35.5, $\Delta G(298 \text{ K})$ +30.5, $\Delta G(350 \text{ K})$ +41.3 kcal/mol. ^c Anion in the N-methyl bay. ^d The ΔE_{el} of -132.1 kcal/mol for the stack with alternating N-methyl and N-butyl occupancy lies in-between the values for the pure stacks, which corresponds well to the weighted average stabilization. ^e Iodide in the N-butyl bay.

Optoelectronic Properties (cyclic voltammetry, UV-vis spectra)

Cyclic Voltammetry

Cyclic voltammetry (CV) was performed on a standard one-compartment, three-electrode cell connected to an Electrochemical Analyzer BAS 100B/W (Bioanalytical Systems). A glass carbon disk of 3 mm diameter was used as a working electrode with a Pt wire as a counter electrode and an Ag/AgCl electrode as a reference electrode. Solvents were obtained from a solvent purification system (Innovative Technology Inc. MA, USA, Pure-Solv 400) and tetrabutylammonium perchlorate (TBAClO₄) of electrochemical grade was used as supporting electrolyte (Aldrich). Ferrocene (Fluka) functioned as internal standard ($E_{1/2ox}$ of ferrocene/ferrocenium in CH₂Cl₂ was 0.48 V vs. Ag/AgCl and set equal to 4.80 eV). All measurements were conducted under dry argon at a scan rate of 100 mV/s. E_{HOMO} was calculated from electrochemical measurements by E_{HOMO} (eV) = $-[E_{1/2} - (0.48 \text{ V})] - 4.8 \text{ eV}$. The reported oxidation potential for I⁻ in aqueous solution is +0.343 V (vs. Ag/AgCl) (+0.54 V vs. SHE) if the potential of the half-cell Ag/AgCl is +0.197 V (vs. SHE).⁵ Twofold oxidation of iodide occurs at +0.98 V (vs. SHE) or +0.78 V (vs. Ag/AgCl).⁵ The oxidation potentials for BF₄⁻ and trifluoromethanesulfonate in propylene carbonate are 3.6 V (vs. SHE) and 3.0 V (vs. SHE),⁶ respectively, which are well outside the electrochemical window of dichloromethane.

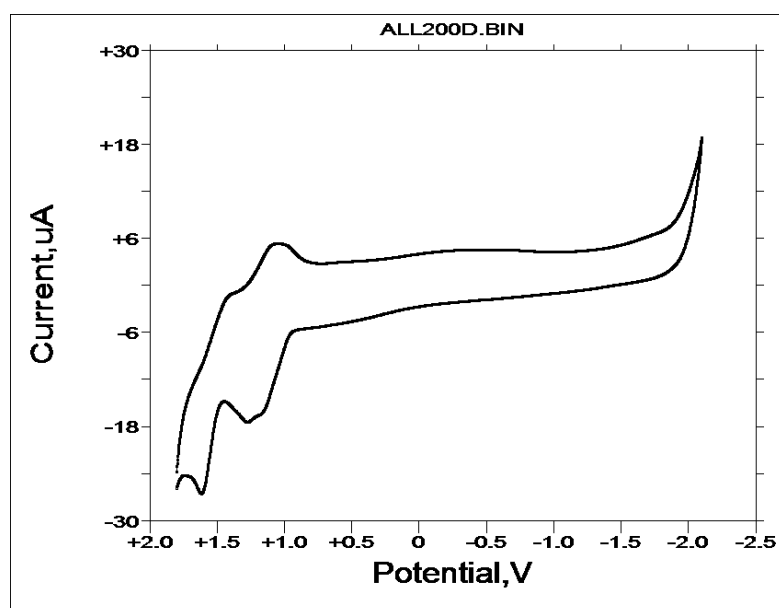


Figure S32. CV of compound **8-6** in 10⁻⁴ M CH₂Cl₂ solution.
 $E_{1/2(ox1)} = +1.07 \text{ V}$; $E_{1/2(ox2)} = +1.53 \text{ V}$
 $E_{HOMO} = -5.39 \text{ eV}$

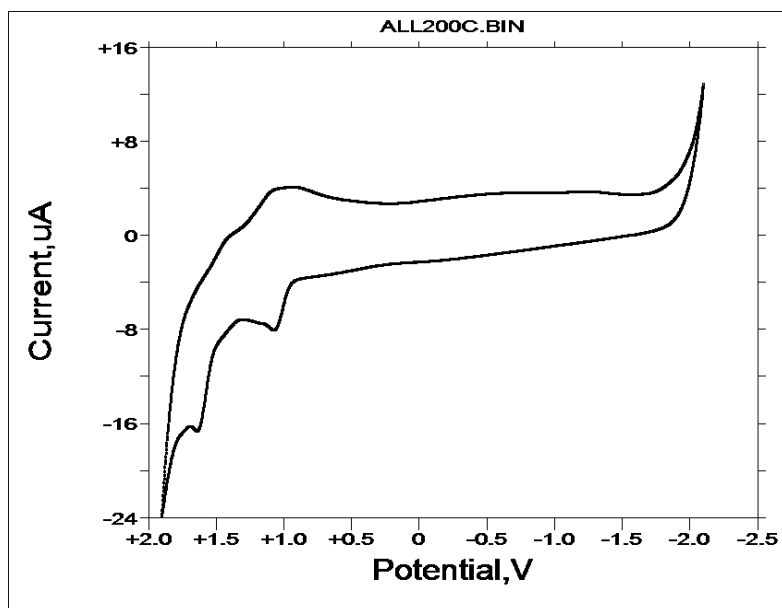


Figure S33. CVs of compound **8-12** in 10^{-4} M CH_2Cl_2 solution.

$E_{1/2}(\text{ox1}) = +1.01$ V; $E_{1/2}(\text{ox2}) = +1.53$ V

$E_{\text{HOMO}} = -5.33$ eV

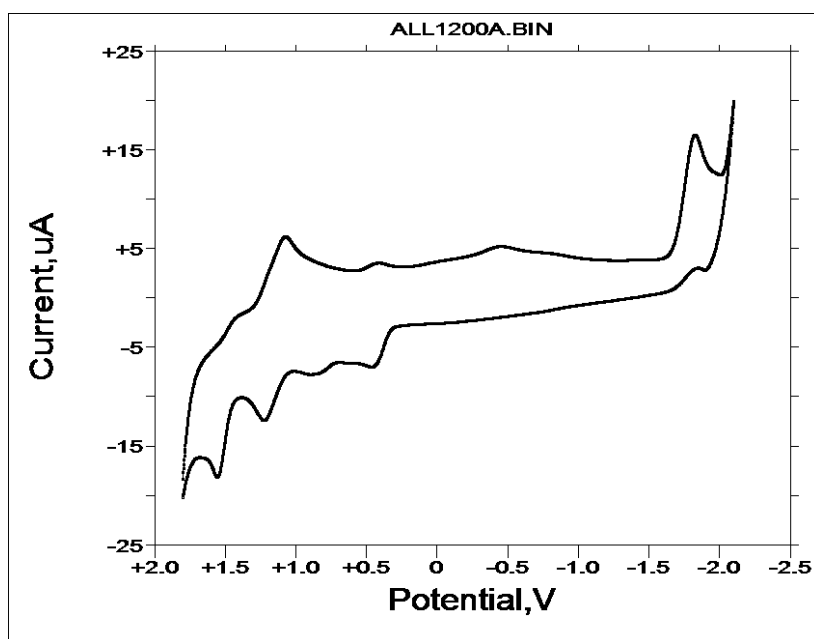


Figure S34. CVs of compound **9-6-I** in 10^{-4} M CH_2Cl_2 solution.

$E_{1/2}(\text{ox1}) = +0.44$ V; $E_{1/2}(\text{ox2}) = +0.81$ V; $E_{1/2}(\text{ox3}) = +1.15$ V; $E_{1/2}(\text{ox4}) = +1.49$ V
(ox1 and ox2 are likely oxidations of iodide)

$E_{1/2}(\text{red}) = -1.86$ V

$E_{\text{HOMO}} = -5.47$ eV (based on ox3);

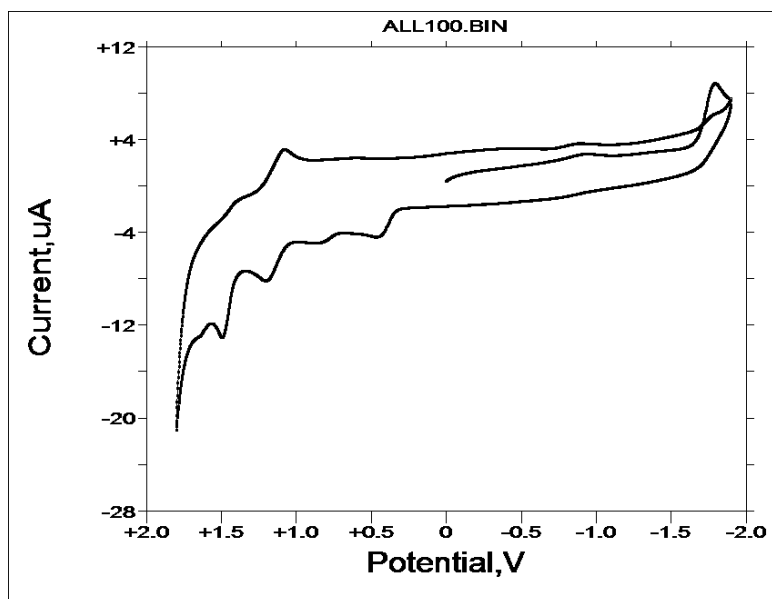


Figure S35. CVs of compound **9-12-I** in 10^{-4} M CH_2Cl_2 solution.

$E_p(\text{ox1}) = +0.45$ V; $E_p(\text{ox2}) = +0.84$ V; $E_{1/2}(\text{ox3}) = +1.13$ V; $E_{1/2}(\text{ox4}) = +1.44$ V
(ox1 and ox2 are likely oxidations of iodide)

$E_p(\text{red}) = -1.80$ V

$E_{\text{HOMO}} = -5.45$ eV (based on ox3);

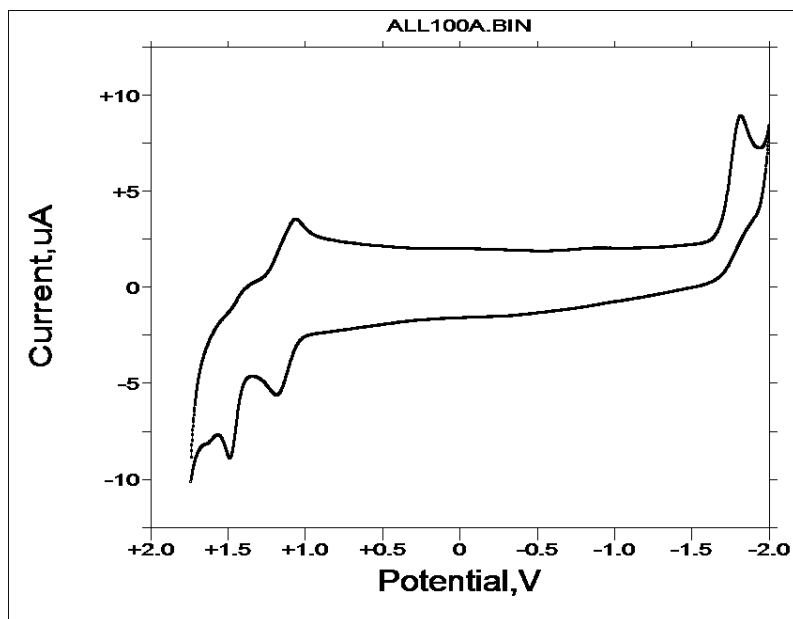


Figure S36. CVs of compound **9-12-BF₄** in 10^{-4} M CH_2Cl_2 solution.

$E_{1/2}(\text{ox1}) = +1.12$ V; $E_{1/2}(\text{ox2}) = +1.44$ V;

$E_{1/2}(\text{red}) = -1.87$ V

$E_{\text{HOMO}} = -5.44$ eV;

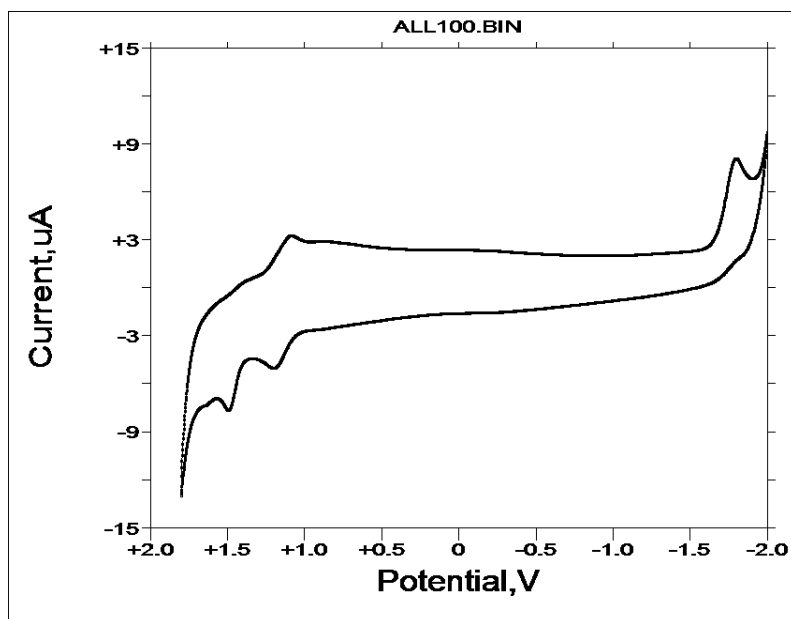


Figure S37. CVs of compound **9-12-OTf** in 10^{-4} M CH_2Cl_2 solution.

$E_{1/2}(\text{ox1}) = +1.14$ V; $E_{1/2}(\text{ox2}) = +1.45$ V;

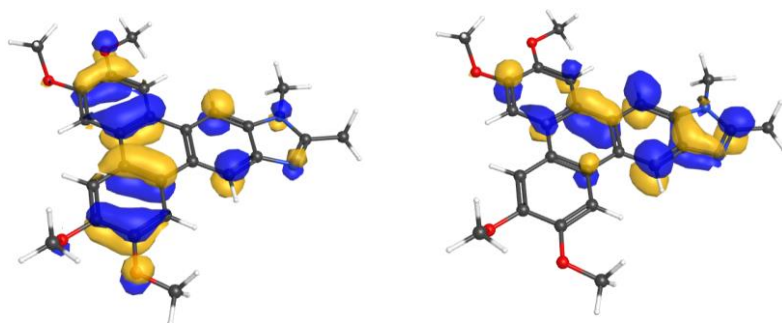
$E_{1/2}(\text{red}) = -1.84$ V

$E_{\text{HOMO}} = -5.46$ eV;

UV-Vis Spectra and Optical Gaps

UV-Vis spectra in THF solutions of 10^{-4} to 10^{-7} molar concentrations were taken with a Bruker Cary 50 spectrometer. The extinction coefficients were calculated as an average of three measurements and no deviations from the Lambert-Beer law were observed for this concentration range. Solutions of about 10^{-4} molar concentration were run in cuvettes of 1 mm instead of 10 mm pathlength. Optical energy gaps (HOMO-LUMO gaps) were estimated from the onsets of absorption.

a)



b)

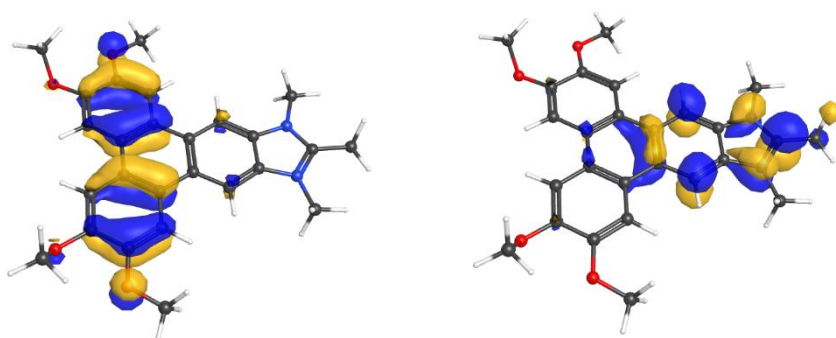


Figure S38. Depictions of HOMO (left) and LUMO (right) for the a) all-methyl **8-1** and b) N-methylated cation **9-1**. From B3LYP/6-31+G(d,p); orbitals from ω B97X-D are virtually identical.

Table S7. Absorption peaks with molar extinction coefficients (ϵ) in $M^{-1}cm^{-1}$. Onsets of absorption were used to determine the optical energy gap (HOMO-LUMO gap).

Compound	λ_6 (nm) (ϵ)	λ_5 (nm) (ϵ)	λ_4 (nm) (ϵ)	λ_3 (nm) (ϵ)	λ_2 (nm) (ϵ)	λ_1 (nm) (ϵ)	Onset (nm) E_{gap} (eV)
8-6	253 (32997)	275 (68006)	283 (95961)	319 (24676)	shoulder	shoulder	374 3.32
8-12	253 (30729)	275 (62153)	282 (85392)	319 (23012)	shoulder	shoulder	374 3.32
9-6-I	253 (52987)	shoulder	281 (77891)	324 (41375)	350 (9903)	369 (7736)	415 2.99
9-12-I	252 (54965)	shoulder	282 (72801)	325 (38596)	351 (9292)	370 (7211)	412 3.01
9-12-BF₄	253 (48921)	shoulder	281 (77656)	324 (35599)	349 (8415)	367 (6257)	409 3.03
9-12-OTs	253 (48920)	shoulder	282 (74012)	324 (37207)	350 (8839)	366 (6781)	413 3.00

References

- S1. S. Chen, F. S. Raad, M. Ahmida, B. R. Kaafarani and S. H. Eichhorn, *Org. Lett.*, 2013, **15**, 558–561.
- S2. J. Charton, S. Girault-Mizzi, M.-A. Debreu-Fontaine, F. Foufelle, I. Hainault, J.-G. Bizot-Espiard, D.-H. Caignard and C. Sergheraert, *Bioorg. Med. Chem.*, 2006, **14**, 4490–4518.
- S3. F. Morale, R. W. Date, D. Guillon, D. W. Bruce, R. L. Finn, C. Wilson, A. J. Blake, M. Schröder and B. Donnio, *Chem. Eur. J.* 2003 (**9**,11) 2484.
- S4. M. Ue, *J. Electrochem. Soc.*, 1994, **141**, 3336–3342.
- S5. Y. Zhao, Y. Ding, Y. Li, L. Peng, H. Ryung Byon, J. B. Goodenough and G. Yu, *Chem. Soc. Rev.*, 2015, **44**, 7968-8378.
- S6. M. Ue, M. Takeda, M. Takehara and S. Mori, *J. Electrochem. Soc.*, 1997, **144**, 2684–2688.
- S7. Gaussian 16, Revision C.01, M. J. Frisch, G. W. Trucks, H. B. Schlegel, G. E. Scuseria, M. A. Robb, J. R. Cheeseman, G. Scalmani, V. Barone, G. A. Petersson, H. Nakatsuji, X. Li, M. Caricato, A. V. Marenich, J. Bloino, B. G. Janesko, R. Gomperts, B. Mennucci, H. P. Hratchian, J. V. Ortiz, A. F. Izmaylov, J. L. Sonnenberg, D. Williams-Young, F. Ding, F. Lipparini, F. Egidi, J. Goings, B. Peng, A. Petrone, T. Henderson, D. Ranasinghe, V. G. Zakrzewski, J. Gao, N. Rega, G. Zheng, W. Liang, M. Hada, M. Ehara, K. Toyota, R. Fukuda, J. Hasegawa, M. Ishida, T. Nakajima, Y. Honda, O. Kitao, H. Nakai, T. Vreven, K. Throssell, J. A. Montgomery, Jr., J. E. Peralta, F. Ogliaro, M. J. Bearpark, J. J. Heyd, E. N. Brothers, K. N. Kudin, V. N. Staroverov, T. A. Keith, R. Kobayashi, J. Normand, K. Raghavachari, A. P. Rendell, J. C. Burant, S. S. Iyengar, J. Tomasi, M. Cossi, J. M. Millam, M. Klene, C. Adamo, R. Cammi, J. W. Ochterski, R. L. Martin, K. Morokuma, O. Farkas, J. B. Foresman, and D. J. Fox, Gaussian, Inc., Wallingford CT, 2019.
- S8. J. J. P. Stewart, *J. Mol. Model.*, 2007, **13**, 1173-213.
- S9. A. D. Becke, *J. Chem. Phys.* 1993, **98**, 5648-5652.
- S10. C. T. Lee, W. T. Yang and R. G. Parr, *Phys. Rev. B* 1988, **37**, 785-789.
- S11. P. J. Stephens, F. J. Devlin, C. F. Chabalowski and M. J. Frisch, *J. Phys. Chem.* 1994, **98**, 11623-1627.
- S12. J.-D. Chai and M. Head-Gordon, *Phys. Chem. Chem. Phys.* 2008, **10**, 6615-20.
- S13. J. Tomasi, B. Mennucci and R. Cammi, *Chem. Rev.* 2005, **105**, 2999-3093.
- S14. T. Singh and A. Kumar, *J. Phys. Chem. B*, 2008, **112**, 12968-12972.
- S14. J. B. Foresman, T. A. Keith, K. B. Wiberg, J. Snoonian and M. J. Frisch, *J. Phys. Chem.* 1996, **100**, 16098-104.
- S15. R. F. W. Bader, *Atoms in Molecules: A Quantum Theory*; Oxford University Press: Oxford, U.K., 1990.
- S16. AIMAll (Version 19.10.12), T. A. Keith, TK Gristmill Software, Overland Park KS, USA, 2019 (aim.tkgristmill.com).
- S17. J. R. Schmidt, W. F. Polik, *WebMO Enterprise*, Version 21.0.010p; WebMO LLC: Holland, MI, USA, 2023; <http://www.webmo.net> (accessed May 25, 2024).
- S18. GaussView, Version 6.1.1, R. Dennington, T. Keith and J. Millam, Semichem Inc., Shawnee Mission, KS, 2019.
- S19. I. Gutman and S.J. Cyvin, *Introduction to the Theory of Benzenoid Hydrocarbons*, Springer, Berlin, 1989.